

26. USE OF GEOPHYSICAL LOGS FOR QUANTITATIVE DETERMINATION OF FRACTURING, ALTERATION, AND LITHOSTRATIGRAPHY IN THE UPPER OCEANIC CRUST, DEEP SEA DRILLING PROJECT, HOLES 504B AND 556¹

Roger N. Anderson, Lamont-Doherty Geological Observatory, Columbia University
Honor O'Malley, Teachers College, Columbia University
and

Robin L. Newmark, Lamont-Doherty Geological Observatory, Columbia University²

ABSTRACT

New analysis and measurement techniques have been developed to extend geophysical logging to the quantitative determination of the extent of fracturing, degree of alteration, and variation in lithostratigraphy of the oceanic crust. In Hole 504B in 5.9-Ma crust on the south flank of the Costa Rica Rift, a borehole televiewer was used to produce a fracture log of the upper crustal Layers 2A, 2B, and 2C. A new differencing scheme was then developed for the determination of the percentage of hydroxyl minerals in the formation from neutron porosity and gamma-ray-density logs. Changes in full waveform sonic-log power spectra of compressional, shear, Stoneley, and normal mode coda correlate with fracture patterns. Only in the sheeted dikes of Layer 2C could quantitative estimation of the fracture aspect ratio be made; Layers 2A and 2B are too heavily fractured and altered. In the pillow basalts of Layer 2A, there is weak correlation between compressional velocity and degree of alteration, with low sonic velocities appearing to be controlled more by extensive, open fractures. Alteration, rather than fracturing, affects velocity in the heavily altered pillow basalts of Layer 2B, however. Within the dikes of Layer 2C, antiresonance is observed in the spectra of compressional- and shear-wave coda in energies of 30–40 cm wavelengths. A model is developed that treats the medium as highly fractured so that fractures intersect the well bore to form "vents." Antiresonances within the vents are then due to a half-wavelength, vent-resonance system. Using this model, fracture lengths are calculated to average about 25 cm in the dikes. Fracture apertures are observed to be 1 to several mm in diameter from the borehole televiewer.

The venting model also accounts for the filter characteristics of the power spectra of the Stoneley and normal mode coda observed in the dike section of Hole 504B. The intervals in which energy levels of Stoneley and normal mode coda are low correlate with zones of intense fracturing observed in the borehole televiewer log. In the highly dispersive normal modes, frequency changes track energy variations. When energy is high in unvented, lightly fractured segments of the borehole, center frequency is high; when energy is dissipated into vents in highly fractured portions of the hole, the center frequency of these low-energy intervals is low as well.

In contrast, geophysical logs from Hole 556 in 17-Ma crust on the west flank of the Mid-Atlantic Ridge clearly indicate major alteration and lithology changes within the 177 m of crust penetrated. Hydroxyl-mineral content and M-N cross plots identify pillow basalt, basaltic breccia, and massive basalt zones, as well as gabbro, gabbroic breccia, and serpentinized gabbro layers found at the bottom of the well. Sonic waveforms respond to impedance changes not only from fracturing as in Hole 504B but from alteration and lithology changes as well. Changes in the power spectra appear to be controlled somewhat by alteration. Relatively fresh basalt and gabbro allow the passage of high energy and exhibit high-frequency compressional and shear coda. The opposite is the case for highly altered serpentinized gabbro and breccia. Serpentinized gabbro acts as a frequency-dependent attenuator. The spectral changes are influenced by the complex reactance of the crust, but too many variables prevent further quantification.

INTRODUCTION

The upper layers of the oceanic crust are characterized by large changes in geophysical properties, both laterally and with submarine depth, that belie their volcanic modes of origin. Feeder dikes connecting surface-flow basalts with the magma chamber below produce new seafloor with similar volcanic structure within the spreading systems active worldwide on mid-ocean ridges. All ocean crust consists of pillow basalts overlying sheeted dikes, which in turn rest upon gabbros that are the frozen remains of old magma chambers. Even the chemistry of the oceanic crust is essentially the same from ocean to ocean. It is the rare ocean basalt that differs

from mid-ocean ridge basalt (MORB), or MORB composition. Yet geophysical properties of Mid-Atlantic Ridge flank crust can be very different from East Pacific Rise crust. For example, the seismic velocity in the uppermost crust is often slower in the Atlantic than in the Pacific (Houtz and Ewing, 1976). The most highly altered metamorphic rocks are invariably found in the Atlantic.

Since the volcanic origin of all seafloor assures similar initial composition and general structure, studies of the causes of geophysical differences quickly lead to interesting conclusions concerning (1) the amount of faulting and fracturing the crust undergoes after emplacement, (2) the degree of hydrothermal circulation and metamorphic alteration the crust experiences during aging, and (3) the permeability structure of the crust that ties 1 to 2. Put another way, physical properties such as the propagation of elastic waves, or the variation in permeability and porosity with depth, are controlled by the degree and interconnectedness of fracturing in the crust

¹ Anderson, R. N., Honnorez, J., Becker, K., et al., *Init. Repts. DSDP*, 83: Washington (U.S. Govt. Printing Office).

² Addresses: (Anderson, Newmark) Borehole Research Group, Lamont-Doherty Geological Observatory, Columbia University, Palisades, NY 10964; (O'Malley) Teachers College, Columbia University, New York, NY 10027.

and by the degree and extent of alteration that metamorphoses the crust and fills the fractures.

Direct determination of sonic velocity, electrical resistivity, and porosity have been made *in situ* in the oceanic crust for several years by geophysical logging in Deep Sea Drilling Project (DSDP) boreholes. In this chapter we report results of several new analysis and measurement techniques that extend geophysical logging through the use of multichannel sonic tools that record multiple seismic waveforms over short intervals, ultrasonic borehole imagers that produce an accurate picture of the well bore, and active nuclear source-counter arrays that separate hydroxyl-mineral content from free-water porosity in the formation. These three techniques are then combined to locate fractures and quantify the extent to which they are filled by alteration products.

We use data from the deepest hole yet drilled into the oceanic crust, Hole 504B, in 5.9-Ma seafloor on the south flank of the Costa Rica Rift, eastern equatorial Pacific, as well as data from Hole 556 in 17-Ma seafloor on the west flank of the Mid-Atlantic Ridge, to demonstrate the applicability of the new techniques for identifying differences in lithology, alteration, and fracturing found in the two oceans. Our ultimate aim is to characterize the permeability, degree of alteration, and structure of these holes hoping to understand the physical and chemical processes that produce very different geology at these disparate sites.

THE EXPERIMENT IN HOLE 504B

In November–January 1981–1982, Leg 83 of the Deep Sea Drilling Project reoccupied Hole 504B on the south flank of the Costa Rica Rift and extended drilling begun previously during Legs 69 and 70 to over 1 km into the upper oceanic crust (Fig. 1). Three layers were drilled: an uppermost rubbly zone made up of intermixed pillow basalts, basaltic breccia, and flow basalts in the form of sills (called Layer 2A); an intermediate zone of more thoroughly altered and cemented pillow basalts (Layer 2B); and a lower unit of sheeted basaltic dikes (Layer 2C). The following Schlumberger well services logs were run over the depth range 274.5–1287.5 m below seafloor, nearly the complete basement section of Hole 504B: active-source neutron porosity and gamma-ray-density logs; spherically focused electrical laterolog; caliper; and four-channel, long-spaced sonic logs (Fig. 2). An additional run of the sonic tool was made that windowed-out the usual first-arrival compressional wave and recorded instead the shear-wave velocity (Newmark et al., this volume). Two additional specialty logs were run in the hole: a large-scale electrical resistivity log (Becker et al., 1982; Becker, this volume), and a United States Geological Survey (USGS) borehole televiewer (BHTV) log (Newmark et al., this volume).

Virtually every log registered a change in gradient (see Newmark et al., this volume) from the Layer 2A pillow basalts in the upper 150 m, to the Layer 2B pillows and breccias of the next 400 m, and finally into the sheeted dikes of Layer 2C over the lower 500 m of Hole 504B (Fig. 2). For example, note the change in slope at 4300 m in the compressional velocity, porosity, and resistivity

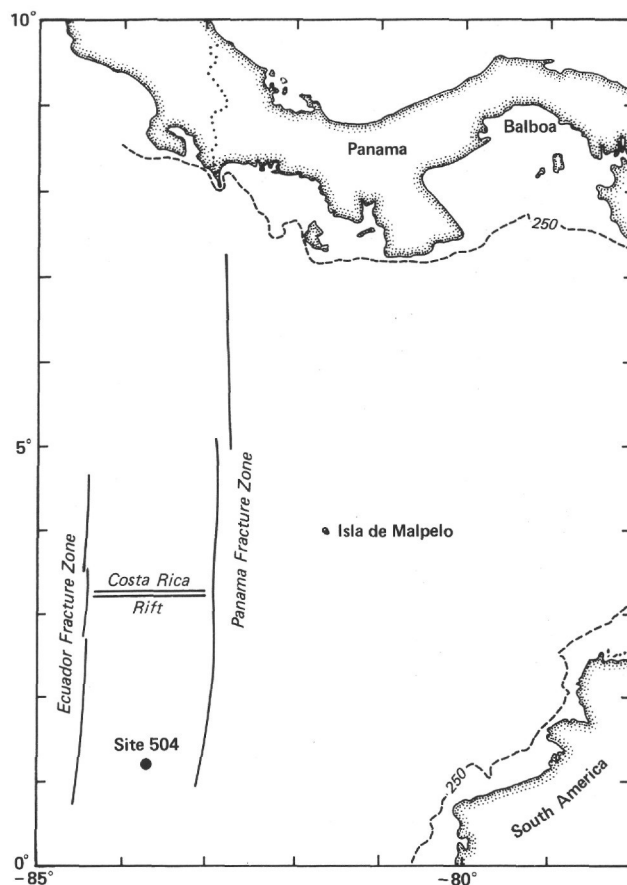


Figure 1. Location of DSDP Hole 504B in the eastern equatorial Pacific.

of the crust. This boundary marks the deepest occurrence of pillow basalts and the first recovery of dikes within the cores in Hole 504B (Anderson et al., 1982).

Estimate of Hydroxyl-Mineral Content

The core recovery within oceanic basement on the Deep Sea Drilling Project averages 30% worldwide. In the sheeted dikes at the bottom of Hole 504B, it falls off to less than 15%. Even when the recovery is excellent, it is not easy to quantify either the amount of alteration or its detailed variation with depth in the crust. Bulk chemical analyses accurately measure hydroxyl-mineral content, but can only be run on a few selected samples from the cores. The active-source nuclear logs offer a method of calculating the quantity of hydroxyl present over the entire well bore length; this is a method soundly based in the nuclear physics of neutron and gamma-ray propagation.

With a method commonly called "density logging," a cesium-137 chemical source is lowered into the borehole and pressed against the wall rock with a hydraulic pad. Medium-energy gamma rays emitted by the source at several hundred keV interact with the formation by Compton scattering with electrons. Two gamma-ray counters spaced 1 and 2 ft., respectively, away from the source on the pad measure the gamma-ray intensity at those points. Two counters allow for the correction for bore-

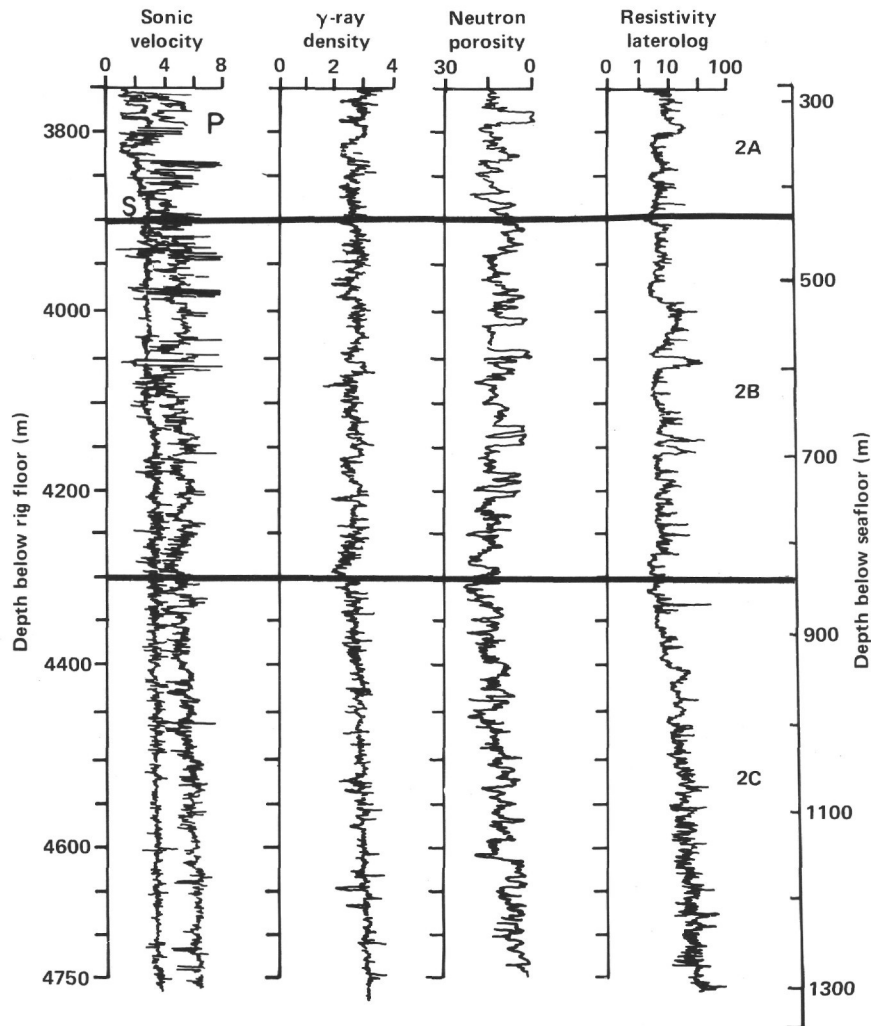


Figure 2. Geophysical logs from Hole 504B. Sonic, nuclear, and resistivity logs were from Schlumberger Well Services. Gradient changes in all the logs at 3900 m (425 m below seafloor) and at 4300 m (825 m BSF) are Layer 2A/2B and 2B/2C boundaries, respectively.

hole geometry effects by differencing the far-field counter and the closest counter, which will be more severely affected by near-field, borehole effects. Compton scattering is not dependent upon specific elements, but upon electron density of the formation.

The electron density of the formation has three components; the bulk density of the rock, the water present as porosity in pore spaces, and the water bound into alteration products as hydroxyls. The density log does not distinguish between the density of the alteration products versus that of unaltered rock. Instead, a bulk density of the formation plus porosity is determined by measuring the formation electron density. Electron density can then be converted to bulk formation density as follows:

$$C \sim I e^{-d RhoB} \quad (1)$$

where

C = count rate

I = a constant related to the strength and geometry of the source

d = a scaling constant

$RhoB$ = formation bulk density.

Since cores recovered on the *Glomar Challenger* are routinely put through a gamma-ray-density measurement in the laboratory aboard ship immediately upon sampling, and since the cored material is representative of the density of the country rock between fractures in the oceanic crust, this laboratory density minus $RhoB$ from the gamma-ray log gives the porosity of the formation. Porosity is calculated as the ratio of Rho measured on cores minus $RhoB$ to Rho measured on cores minus Rho seawater, since seawater is both the drilling fluid and the approximate composition of the formation fluid in pore spaces. The density log measures the porosity of the formation accurately, but does not determine hydroxyl-mineral content, which would contribute to lowered density measurements of the laboratory samples.

Separately, an americium-beryllium neutron source is mounted with two helium-3 neutron detectors on another skid pad within the nuclear tool configuration and run downhole as well. This source emits fast neutrons

with average energies of about 4.5 meV. These neutrons are scattered and lose energy during collision with formation nuclei. Energy loss is inversely proportional to the mass of the struck nucleus. Stated simply, when a neutron hits something its own size, maximum energy transfer occurs. By analogy, if a marble hits a bowling ball, little energy is transferred. However, if a marble hits another marble its own size, maximum energy transfer occurs. Hydrogens have mass approximately equal to neutrons, and their mass is much less than any other element in the formation; so if we measure the energy state of near-field and far-field neutron counters (for borehole size compensation), we have a quantitative measure of the total number of hydrogens in the formation. Hydrogen present as hydroxyl in alteration minerals is measured just as accurately as hydrogen in free water in pore spaces. The neutron log then gives a fair representation of water present as porosity plus that bound chemically as hydroxyls within alteration minerals.

Commercial logging services offer methods of calculating hydroxyl-mineral content from various cross-correlation techniques involving the entire suite of geophysical logs. Even though we recover only 15–30% of the rock cut by the bit, chemical analyses of these cores place a lower limit on the alteration present in the crust (it is assumed that the hardest, least-altered rock is preferentially cored whereas the highly altered rock crumbles before the drill bit). The alteration content from the neutron and active gamma-ray logs using the commercial “dual-water model” was first calculated for Hole 504B, (MSI, or minimum shale index in Fig. 3). This curve is calculated from an average of neutron and density log porosities (NPHI and DPHI) at each depth point. The lesser of two values, this average (called PHIA) or neutron porosity alone (NPHI), is selected at each point to construct the MSI curve.

This curve did not resemble the degree of alteration observed in the borehole cores (Fig. 3). Specifically, a mineralized stockwork was drilled at 4225–4300 m below the rig floor. This stockwork was composed of up to 60% hydroxyl minerals. However, the MSI curve shows this zone to be unremarkable. Also, the cores reveal that alteration steadily increases from Layer 2A through Layer 2B to peak at the stockwork. The MSI curve does not show such an alteration increase (Fig. 3).

The averaging and minimizing scheme that results in the MSI curve does not make physically sound use of the differences between porosities detected by the neutron versus gamma-ray counters, because it averages these two curves. We have devised a differencing scheme to identify hydroxyl-mineral content of the formation, as follows:

$$\begin{aligned} X &= \text{NPHI} - \text{DPHI} \\ \text{RGHAX} &= (1 + 1.71[1 - 2\text{PHIA} + \text{NPHI}] / (1 - X)) \\ \text{SHLNX} &= (\text{RGHAX} - \text{GDCL}) / (\text{GDSH} - \text{GDCL}) \\ \text{NDI} &= \text{SHLNX} \times (2 - \text{SHLNX}), \end{aligned}$$

where NPHI = neutron porosity; DPHI = gamma-ray density porosity; PHIA = (NPHI + DPHI)/2; GDCL = density of clean, unaltered rock; GDSH = density of

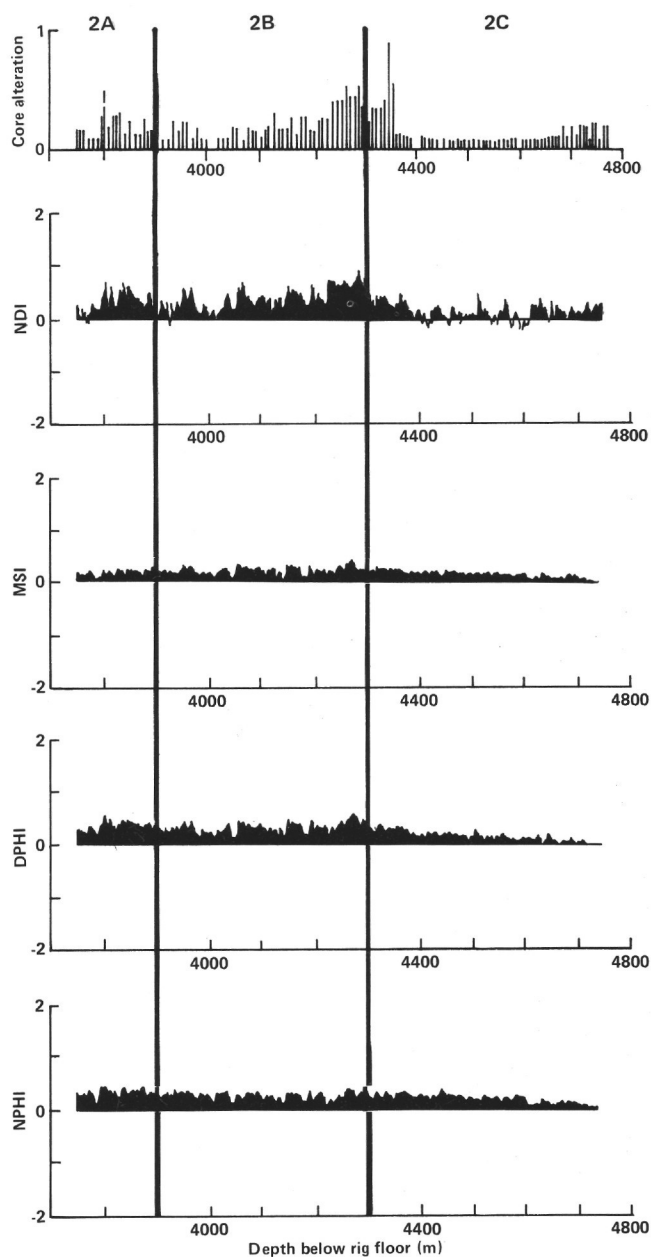


Figure 3. Average values in Hole 504B for NPHI (porosity calculated from the neutron log), DPHI (density calculated from the gamma-ray density log), MSI (minimum shale index from a dual-water CYBERLOOK program), NDI (hydroxyl-mineral content calculated from the differencing scheme; see text), and core alteration. The last histogram was determined from least altered (0) to most altered (1), using visual descriptions from barrel sheets.

alteration material; and NDI = neutron density log index of hydroxyl-mineral content.

We distinguish NPHI and DPHI and scale to the hydroxyl-mineral percentage present in the rock using the lab-log density difference. Our alteration curve faithfully reproduces both the extent of alteration within the stockwork and the increase in hydroxyl-mineral content toward the bottom of Layer 2B (Figs. 2, 3). A slight increase in alteration at the base of the dike sequence is also seen both in our curve and in the cores (Alt and

Laverne, this volume). Our curve is for 100% of the well bore whereas the cores represent less than 15%.

Fracture Log from the Borehole Televiewer

Fractures intersecting the borehole are clearly seen by the BHTV as are the ultrasonic acoustic reflectivity changes that are useful for identification of void spaces and pillow boundaries (Zoback and Anderson, 1982). Fractures were counted in 1-m overlapping intervals down the hole. A "wobble" display of these and the apparent reflectivity of the formation as measured by a photographic light meter are shown in Figure 4, along with the other logs run in the hole. A discussion of the BHTV fracture and reflectivity log as well as the well bore images appears in Newmark et al., this volume.

Zoback and Anderson (1982) found that over the uppermost 500 m of the hole, the intensity of observable fracturing imaged by the televiewer actually increased, in contrast to hypotheses that burial pressures would close fractures as lithostatic pressure increased. They further found that an increase in sonic velocity with depth correlated with an increase in clay in-filling of these fractures instead of with a decrease in the degree of fracturing.

We have extended the Zoback and Anderson (1982) analysis another 500 m into the sheeted dikes of Layer 2C and find that in the dikes the degree of fracturing does begin to decrease as does the amount of alteration (Fig. 4). A corresponding increase in the sonic-velocity gradient accompanies these decreases in fracturing and alteration level, but we doubt these changes are related to the closing of fractures by increase of overburden pressure. Rather, a lower degree of primary fracturing upon cooling is likely.

It should be emphasized, however, that the BHTV sees only large fractures with apertures at least 1 mm wide. The extent of microfracturing often seen in cores returned to the surface from the oceanic crust never shows on BHTV logs. To the first order, the correspondence between fracture and alteration changes seen in the logs and seismic and sonic-velocity gradients observed in the crust suggest that macro- rather than microfractures affect these velocity determinations. The similarity of velocities determined from the very different wavelengths of seismic and sonic energy transmission led Moos and Zoback (1983) to a similar conclusion in wells drilled through crystalline basement on land.

GEOPHYSICAL LOG CROSS-CORRELATION USING THE PHASE DIFFERENCE TECHNIQUE

Now that we have developed the methodology for the determination of quantitative measures of the change in extent of fracturing and degree of alteration change in the borehole, we can then turn to the correlation of these geological processes to the geophysical observations made in the well. For example, qualitative correlation can be seen between the extent of fracturing and degree of alteration in the hole and variations in all the other logs. The gradient change at the Layer 2B/2C boundary is seen both in the BHTV logs and in the alteration content log (Fig. 4).

Another qualitative correlation that is obvious from a visual inspection of the log results is that the amount of attenuation apparent in the sonic waveforms is related in some manner to the degree of alteration seen in the borehole by the nuclear-tool differencing scheme (Fig. 5). Consider the sonic waveform change at 4050 m, or approximately 575 m BSF. Here, a massive, solid flow basalt has little hydroxyl-mineral alteration, and the waveforms are much higher in amplitude with a longer wavetrain than above or below. But the amount of "clay" also correlates somewhat with the fracture-count log from the televiewer (e.g., at 4300 m or about 825 m below seafloor, where a drop in degree of fracturing corresponds to a drop in clay content as well). So are the waveform changes that we see responding to alteration changes downhole, or to fractures, or to fractures filled with clay? If we could determine which, we would have a powerful new diagnostic tool for use in oceanic crust.

Phase Difference

A method is needed to cross-correlate two logs with variable degrees of correlation at different wavelengths down the well. We know that the various logs show a gradient change at the Layer 2B/2C boundary, so they would all correlate strongly at wavelengths approaching the depth of the well (500–1000 m wavelengths). The question of interest here is how well the various logs correlate at the shorter wavelengths at which changes in the degree of fracturing or alteration occur in the formation. We can place a lower limit on our scale of detection because heave of the ship produces inaccurate depth determinations at wavelengths of a few meters and smaller. Cross-correlation at these small wavelengths is hampered by inaccurate depth location.

A technique producing a quantitative correlation coefficient at each wavelength between two wavetrains is phase difference (Newmark et al., this volume, chapter appendix). This method is only useful for portions of logs where it is suspected that one process is affecting two logs to be cross-correlated. Fast-Fourier Transforms (FFT) of the two wiggle plots versus depth are taken. Then the *phase at each wavelength* between two curves is compared. The percentage of correlation between phases is then displayed at each wavelength. Wavelength here is a harmonic of the length of well under consideration. At each wavelength with 50% phase difference, the two curves are in phase half the time and out of phase half the time. This corresponds to a random correlation coefficient of 0.0. If the two curves are exactly in phase all the time, the phase difference at all wavelengths is 100%, or the correlation coefficient is 1.0. If, however, the two curves are exactly out of phase everywhere, then the phase difference is 0%, which corresponds to a correlation coefficient of -1.0 .

The phase difference method first breaks each log into its harmonic components, then correlates each wavelength sequentially, displaying the correlation coefficient at each wavelength as a percentage. The correlation coefficients are then connected by a line to present the degree of correlation over the complete suite of wavelengths contained within the two logs. Thus, if over all wave-

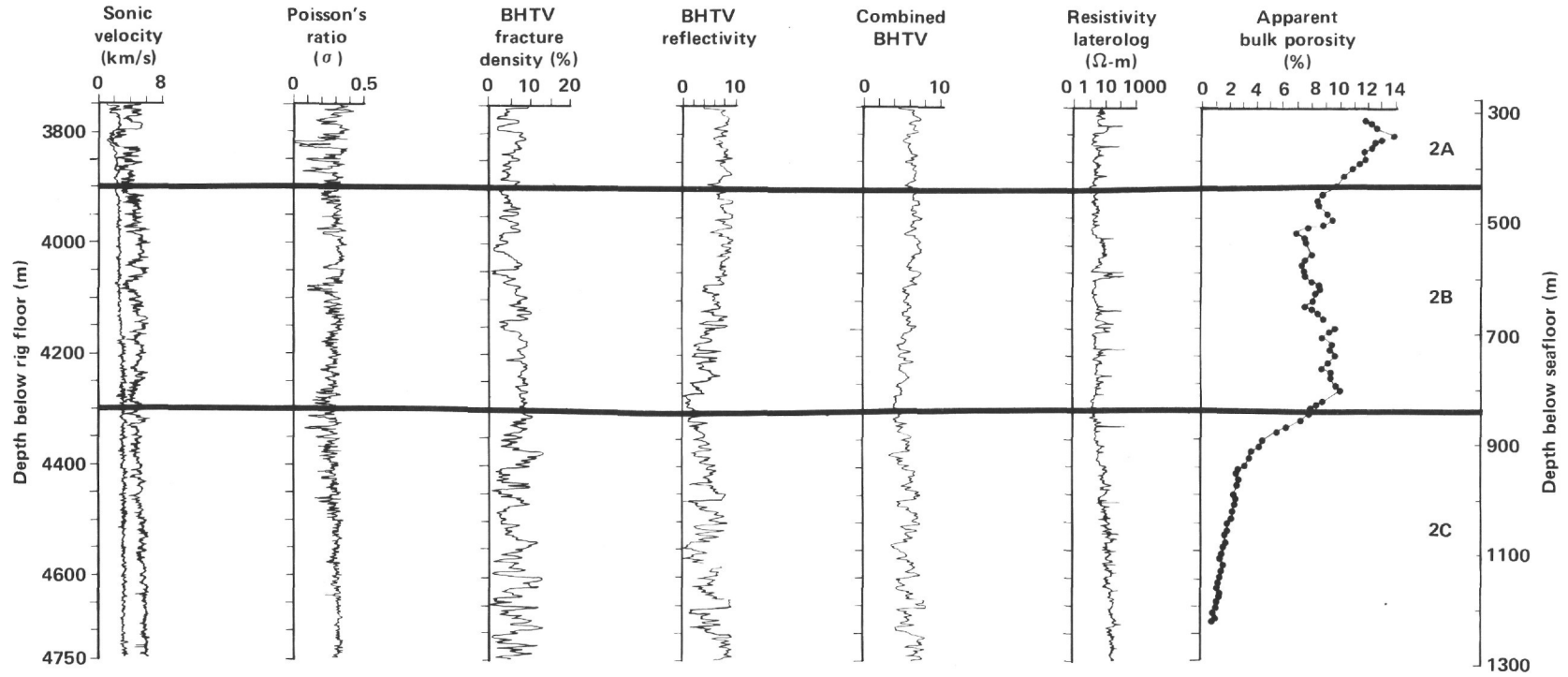


Figure 4. Specialty logs from Hole 504B. Poisson's ratio calculated from compressional and shear velocity logs. BHTV logs were from a United States Geological Survey borehole televiewer (Newmark et al., this volume). Apparent bulk porosities were calculated from large-scale resistivities (Becker et al., 1982; Becker, this volume).

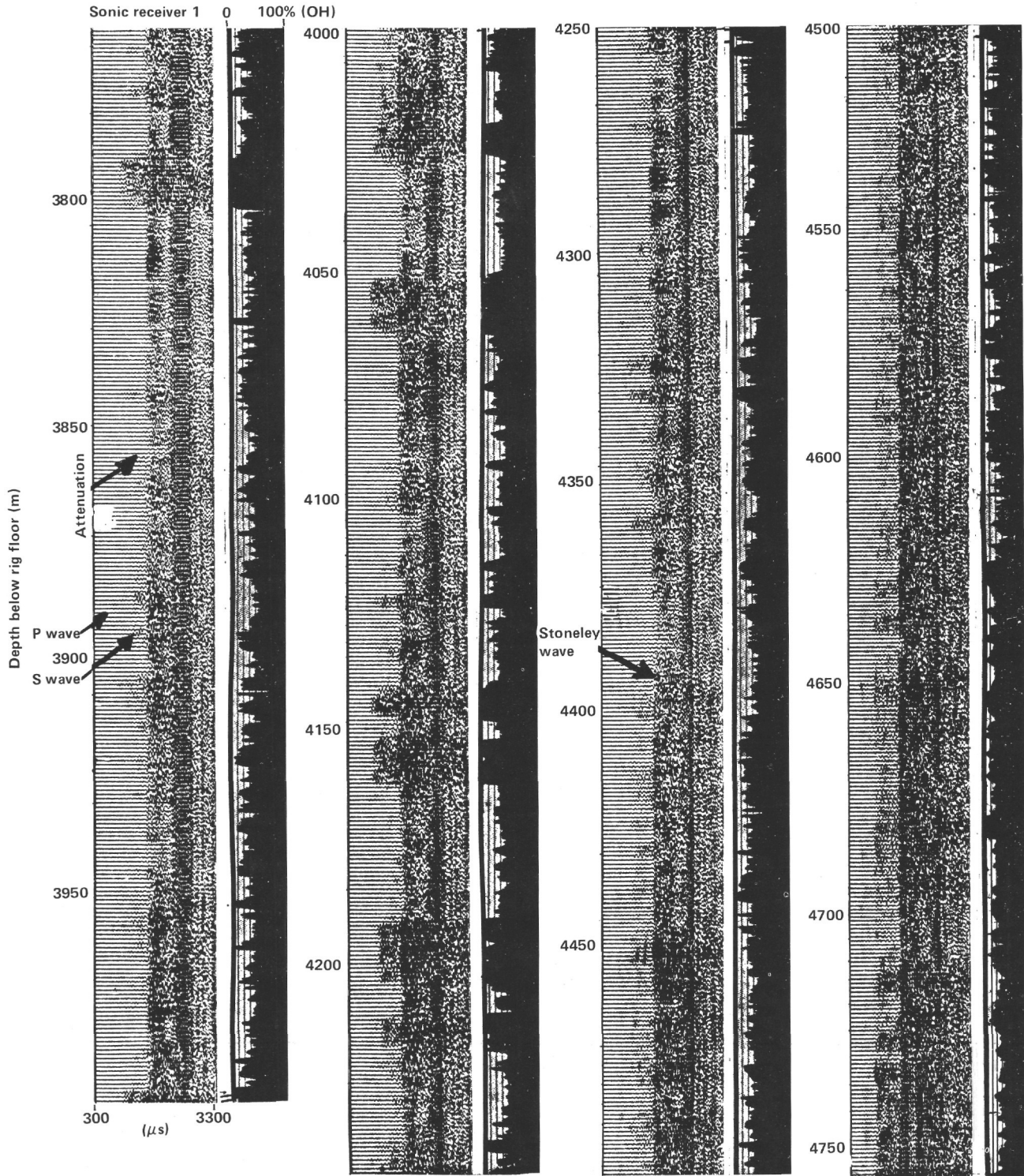


Figure 5. The raw sonic waveforms from the first receiver located 8 ft. above the source are correlated with the hydroxyl content log NDI from Figure 3. Blackness in the last curve is the percentage of matrix material, horizontal bars are every 10% of alteration products present (e.g., at 4100 m depth, 30% altered clays and zeolites, and 70% unaltered basalt are present in the rock).

lengths the correlation is 50%, then the two curves in question are randomly related.

Now consider the pillow basalts in Layers 2A and 2B of Hole 504B. We can question whether there is correlation between alteration content and velocity in Layers

2A and 2B, as might be indicated by Figure 5. First, the phase difference between alteration in these layers and the fracture pattern shows only random correlation at all wavelengths (Fig. 6). Such a truly random-number-generated set of curves for the 550-m interval under ques-

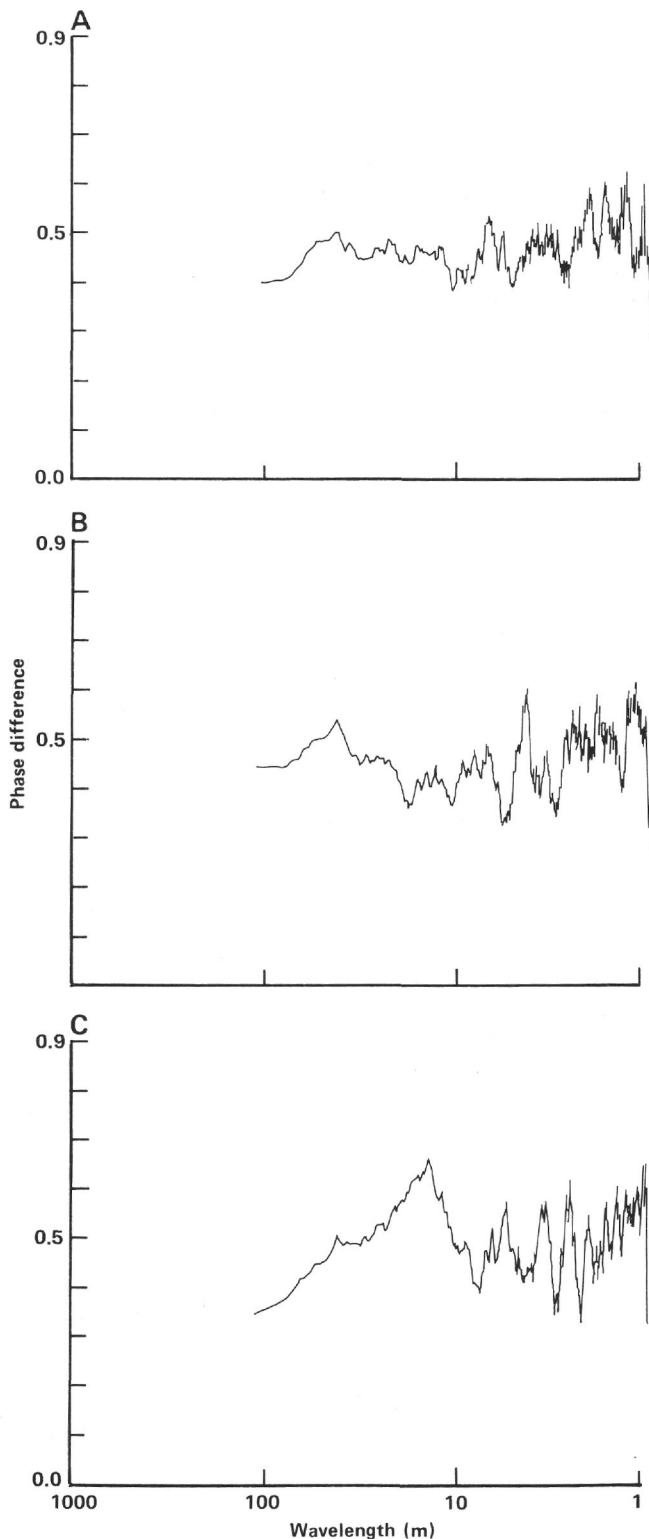


Figure 6. Phase difference analysis (see text) of the cross-correlation of (A) alteration content and fractures derived from borehole televiewer combined BHTV logs, (B) alteration content versus shear wave velocity, and (C) alteration content versus compressional wave velocity. Phase difference method fits FFT harmonics to depth curves in Figure 4, then determines the degree to which two curves are in phase at each wavelength. Wavelength is depth in the hole in meters. 50% correlation is random.

tion shows that we should ignore wavelengths of greater than 100 m (Newmark et al., this volume). At harmonics with 100–550-m wavelengths, there are not enough cycles to give accurate phase difference information. Ship's heave and other depth-determination inaccuracies between different logging runs makes wavelengths less than about 5 m inaccurate as well.

Shear-wave velocity also is randomly correlated with alteration content, but compressional velocity shows weak positive correlation at 10–15-m wavelengths and weak negative correlation at 50–100-m wavelengths (Fig. 6). We expect the effect of alteration to be to lower the velocity of rock, but Zoback and Anderson (1982) showed that velocity increased from Layer 2A into Layer 2B in Hole 504B. They concluded that this observation derived from the fact that the upper crust was heavily fractured, with open porosity in Layer 2A, but lower porosity in Layer 2B caused by increased filling of fractures by alteration products. Porosity is a third variable missing from the analysis in the plots of Figure 6. The phase difference method requires only two independent variables.

Bandpass Filtering

We can isolate the alteration effect on velocity by removing the effects of the large porosity drop in Layer 2A. We accomplish this by removing the trend of both the velocity and alteration content curves, then bandpass filtering the detrended data sets to pass only the long wavelength harmonics. From the phase difference plot (Fig. 7), we place the bandpass filter designed to bring out possible negative correlation between alteration and compressional velocity at 50–150-m wavelengths only (Fig. 7). Use of detrended data at long wavelengths eliminates the positive correlation caused by decrease in porosity over Layer 2A and reveals the extent to which low-velocity zones correlate with zones of high-alteration mineral content (velocity decreases upward in Fig. 7). As can be seen, this correlation is predominant in

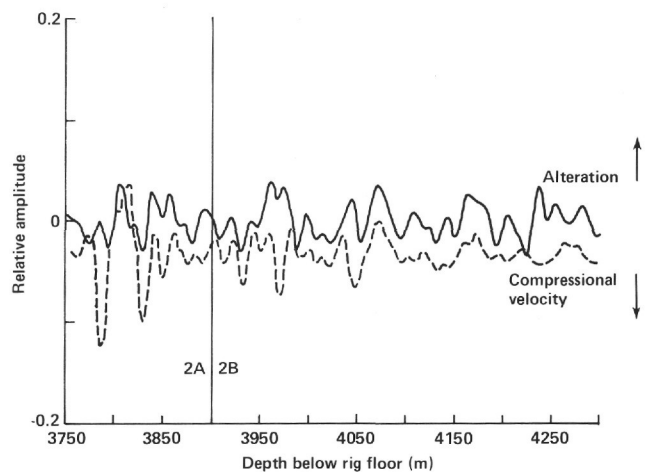


Figure 7. The compressional velocity (Fig. 4) and alteration content (Fig. 3, NDI) are normalized, detrended, and bandpass-filtered to display only wavelengths between 50 and 150 m. The alteration curve has been inverted to show correlation in Layer 2B between high velocities and zones of high alteration mineral content. Arrows indicate the directions of increasing values of each curve.

Layer 2B and much poorer in Layer 2A. It appears that 50–150-m wavelength variations in compressional velocity in Layer 2B are caused by variations in the degree of alteration, as suggested by Zoback and Anderson (1982).

POWER SPECTRA, ATTENUATION, AND FRACTURING IN THE DIKES OF LAYER 2C, HOLE 504B

The sonic waveforms contain much more information about the geology of the rocks through which they pass than just velocity. The sonic-logging tool has a source that emits a broadband acoustic click with significant energy from 15 to 32 kHz. The energy travels from the tool through the borehole drilling fluid (seawater in DSDP holes) as a compressional wave. Upon contact with the well bore, complex waveform conversions occur. Major compressional and shear headwaves propagate into the formation, but the largest energy propagates along the well bore as a tube wave called the Stoneley wave (analogous to the Rayleigh wave except that the Stoneley wave travels along a rock–liquid rather than rock–air surface). Fluid waves called normal modes travel down the borehole as well.

Fracture Spectrum of the Oceanic Crust

To extract more quantitative information about what exactly the sonic waveforms are responding to, we took a Fast Fourier Transform (FFT) of compressional and shear waveform energy packets called “coda” (Fig. 8). The Schlumberger full waveform sonic-logging tool used on DSDP Leg 83 returns waveforms recorded at 8-, 10-, 10-, and 12-ft. spacing from source to receiver. The duplication is required because two different sources are used, although they are acoustically paired as closely as possible. The “shear coda” contains not only a shear wave but other surface waves as well, such as a pseudo-Rayleigh wave, which is about 5% slower than the shear wave, but faster than the Stoneley wave (Richards, personal communication, 1984).

By placing time windows across the waveforms so that first the compressional and then the shear coda can be isolated, power spectra of each coda from four waveforms can be determined at each depth interval down the well. It is then necessary to determine particular frequencies among the waveforms that might be noisy and eliminate spurious energy from the analysis. This “noise” is of unknown origin; some possible known causes are roughness of the well bore, mechanical banging of the tool centralizers against the rock, conversion interference, coupling changes, or geological variations. The spacing between receivers is 2 ft., so we arbitrarily discriminate against differences in the spectra that occur over intervals of less than 2 ft., even if caused by real geology. We calculate the cross product of the FFT of four pairs of waveforms at each depth. The technique calculates the power spectrum of each waveform of the pair, emphasizing frequencies having large amplitudes common to both waveforms. That is, the cross-correlation passes common energy in the time domain.

We then display the wideband *integrated energy* in decibels (dB) between 10 and 20 kHz of each waveform

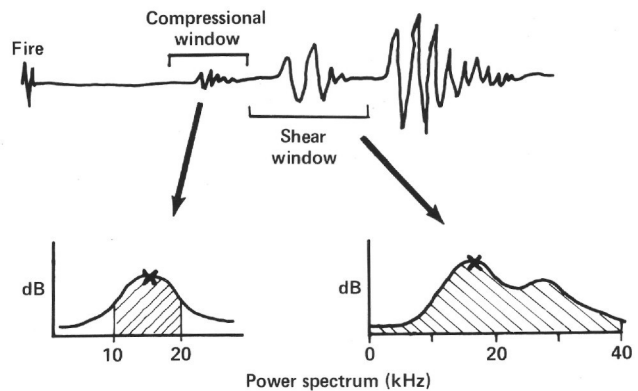
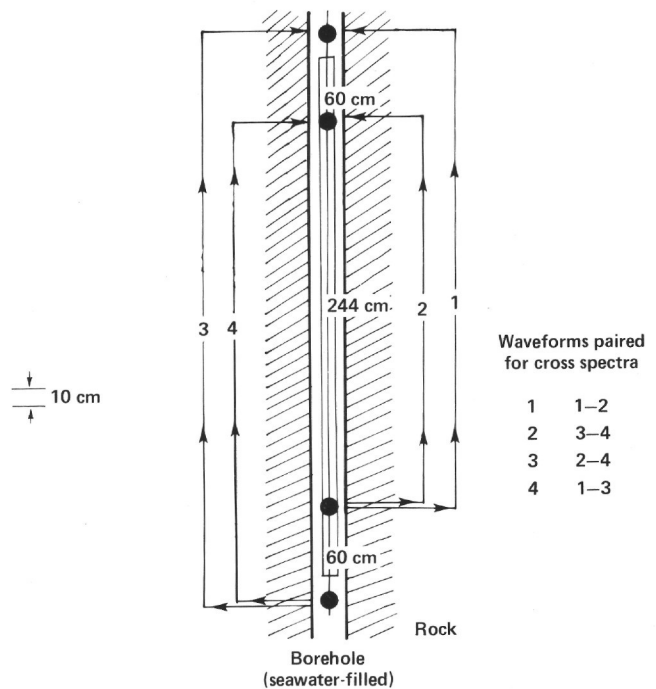


Figure 8. Schematic of Schlumberger sonic-logging tool (SLS-5 4-channel long-spaced sonic sonde) an analysis technique used, first to window waveforms then to calculate the cross spectrum of waveform pairs. This technique was used in both Holes 504B and 556 in the Atlantic. X = center frequency.

spectrum, and energy of peak cross-spectral frequencies as wiggle plots versus depth. We also display the spectra and cross spectra on grayness plots (the greater the energy in decibels at each frequency, the blacker the image) (Figs. 9A, B, C). We show both compressional and shear slownesses ($\mu\text{s}/\text{ft.}$) as well. *Center frequency* is automatically picked and marked by a white bar on the grayness plot. Again, for information, BHTV images are shown in Figure 9 for selected portions of the hole.

This cross-spectral technique shows dramatic variations up and down the hole. Specifically, the entire pillow basalt interval has too low cross-spectral energy on all receiver pairs to yield consistent velocity estimates among all waveform pairs. We require an integrated energy of at least 20 dB above background noise level from the cross spectra or we consider the individual spectra to

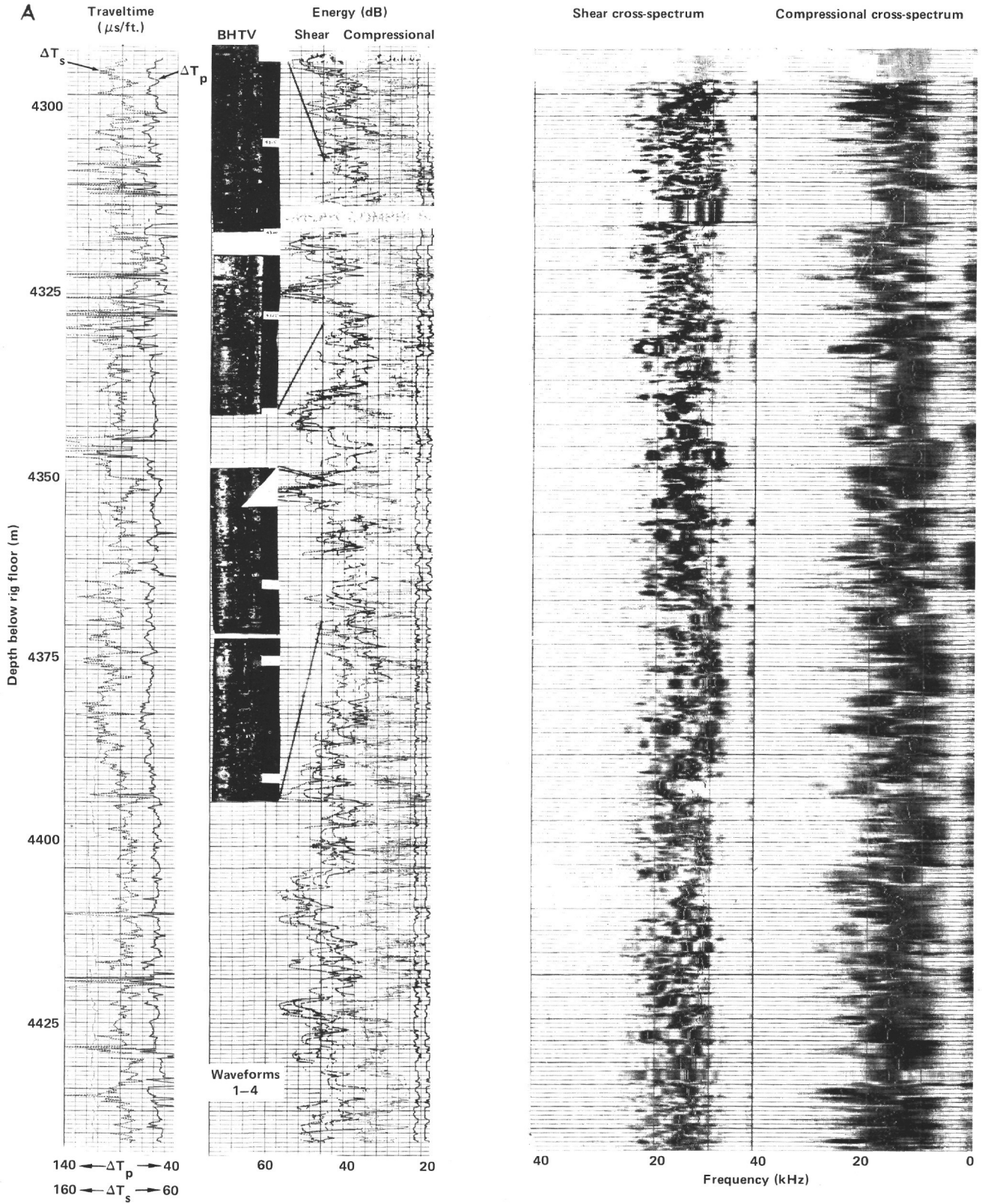


Figure 9. Integrated energy of windowed P-wave and S-wave coda displayed for all four cross-spectral pairs as in Figure 8 in the dikes of Hole 504B. On the right is the actual spectrum at each depth with grayness keyed to power in decibels. The white tick at peak power is the center frequency. On the left, representative BHTV images (Newmark et al., this volume) are displayed. In 9C, four zones are identified in which major changes in energy and center frequency (γ) can be related to televiewer indicated zones of fractures. In Figure 9D, stylized schematic power spectra of compressional and shear energy in Zones 1-4 are shown. QDTP and QDTS are error estimates from cross spectra.

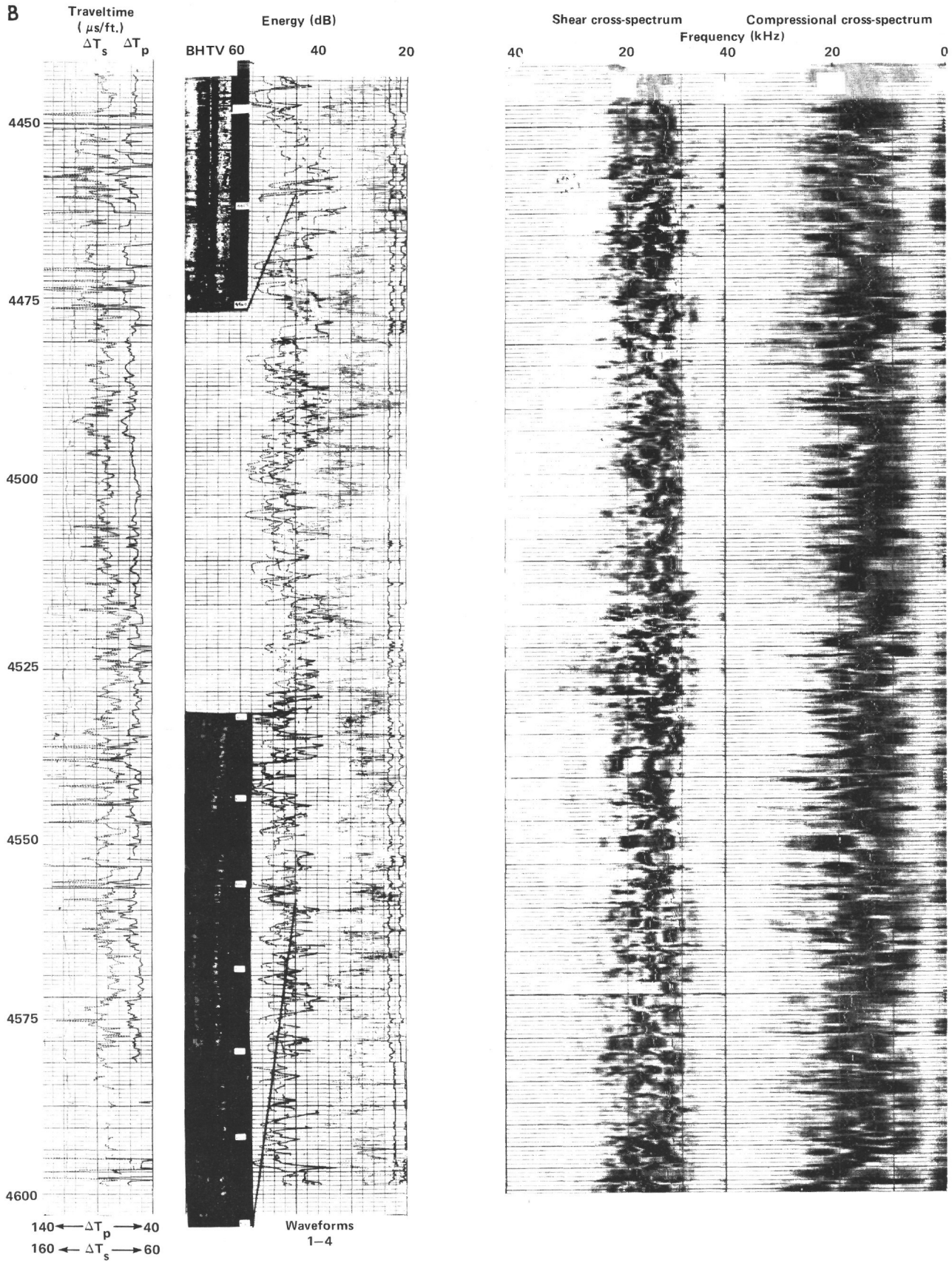


Figure 9. (Continued).

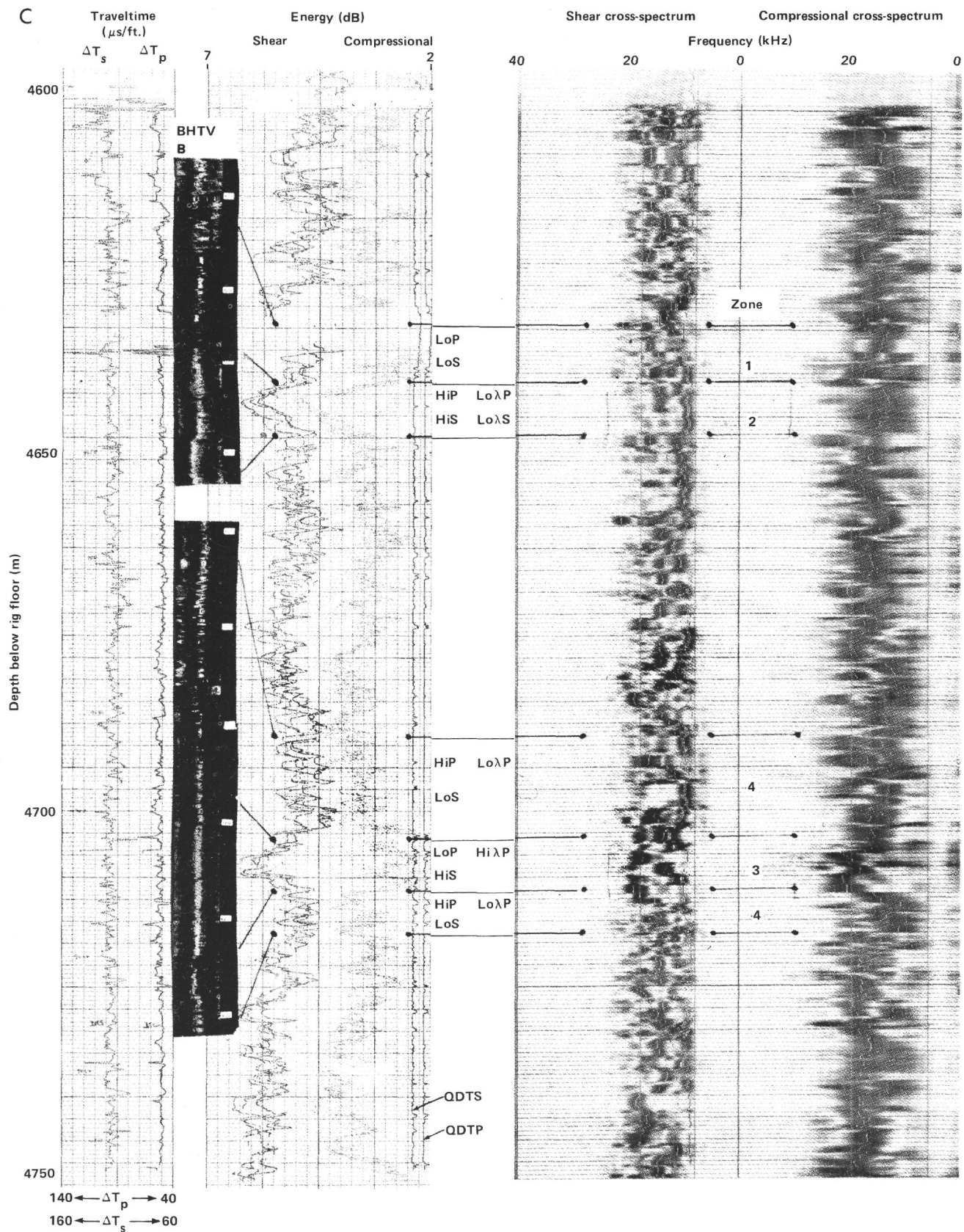


Figure 9. (Continued).

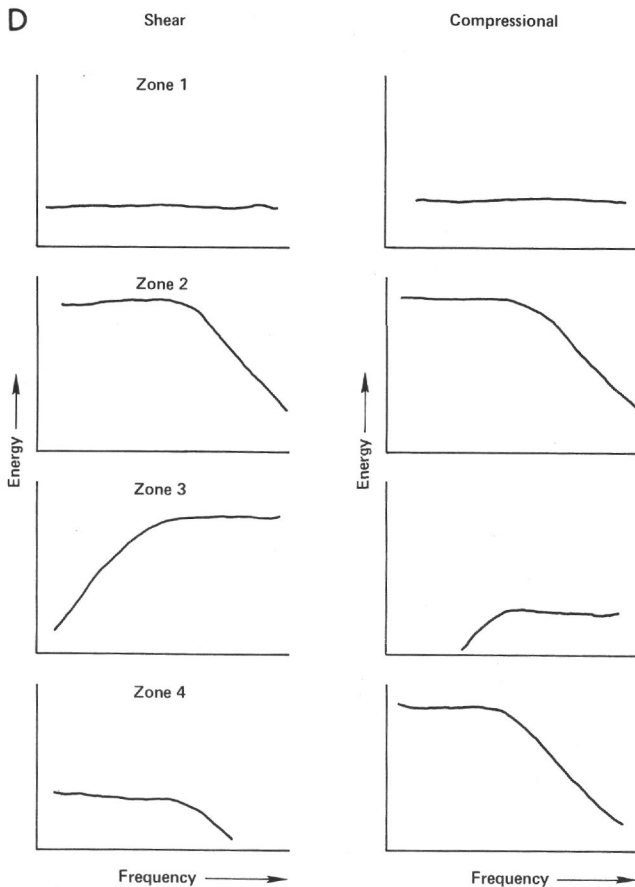


Figure 9. (Continued).

be too different to yield useful cross-spectral information. A partial explanation for this observation is that fracturing and zones of alteration vary too greatly on a scale smaller than the 2-ft. sampling interval so that the sonic receivers record very different waveforms. Consistent first-motion detection required by the slowness estimator was also difficult to achieve. A sonic tool using many more than four receivers spaced at closer than 2-ft. intervals will be required to quantify sonic spectral changes in Layers 2A and 2B of the oceanic crust in Hole 504B.

However, in the dikes at the bottom of Hole 504B, there are significant energy and frequency shifts that must be explained. Consider for example, Zones 1–4 in Figures 9C and 9D: Zone 1 has low P (compressional) and S (shear) energy levels at all frequencies; Zone 2 has high P and S energy, but at low frequencies; whereas Zone 3 has low P energy at high frequencies, but high S energy also at high frequencies; and Zone 4 has high P but low S energy, both at low frequencies.

What causes these energy shifts? If we examine the qualitative correlation with BHTV imagery, we can find a possible solution. For example, Zones 2 and 3 both appear as solid, highly reflective rock on the televiewer image (Fig. 9C). Yet Zone 2 appears to have several large fractures crosscutting the image (black horizontal lines), whereas Zone 3 rock has few fractures. Again Zones 1

and 4 look alike in that both are mostly low-reflectance, highly fractured (altered) rock.

The problem becomes more interesting when we consider the frequency shifts accompanying the energy changes. Consider Zones 2 and 3 again. Zone 2 with its large fractures and high energy levels has very low P and S center frequency, particularly when compared to Zone 3 (Fig. 9D). The scattering effect of large fractures in crystalline media should act as a low-pass filter (e.g., Menke, 1983), and this high-energy but low-frequency behavior within Zone 2 seems to be from such a *low-pass filter*. Zone 3 is dominantly high-frequency P, but has low P-energy levels as well; and shear energy is high at high frequencies. Zone 3 is being *high pass* filtered. No fractures are evident in the televiewer log. By contrast, Zone 4 has low S energy and also low S frequency, but has high P energy at low frequencies, as if from a low-pass filter (Fig. 9D). What physical property could be causing the impedance changes resulting in some zones being high-pass filtered, but others being low-pass filtered?

Another interesting observation from the cross spectra is the resonance character of the borehole/rock system. The compressional cross spectra show resonance about a clearly defined center frequency, but the shear spectra are very different. Multiple resonances are seen throughout the dike interval, particularly in highly attenuated zones (e.g., in Fig. 9C, single-peaked resonance is found in Zone 2, but multiple resonances are found in Zones 1, 3, and 4).

It becomes quite apparent that a means of systematically examining the relation of fractures to the cross spectra must be devised if we are to make much sense of the changes in the waveform spectra. For this purpose, we constructed a "fracture-spectrum" log (Fig. 10). Here we display percent fractures as a wiggle plot versus depth not only with P and S velocity and caliper, as in Figure 2, but with P and S integrated energy and center frequency plotted as well. We take the center frequency within zones of multiresonance as the frequency at which the highest energy occurs, regardless of the energy lobe within which it occurs (Fig. 8).

First, we find no correlation between compressional and shear coda center frequency or energy and caliper log variations (Fig. 11A). We do find correlation between coda-energy and borehole fractures from the televiewer log, however. We can verify that this correlation exists even though the data are variable by again using the phase difference technique (Fig. 12). In these phase difference plots, positive BHTV correlation with high P and S energy is found in zones in Layer 2C; this translates to a correlation between depths with high P- and S-energy levels and zones with a small degree of fracturing from the BHTV log (i.e., the fracture log has been reversed so that zones of fracturing are negative numbers and zones of solid rock are positive numbers. Thus, positive correlation implies high energy at zones of low fracturing.

We find no correlation between degree of alteration and compressional and shear coda energy in the dikes

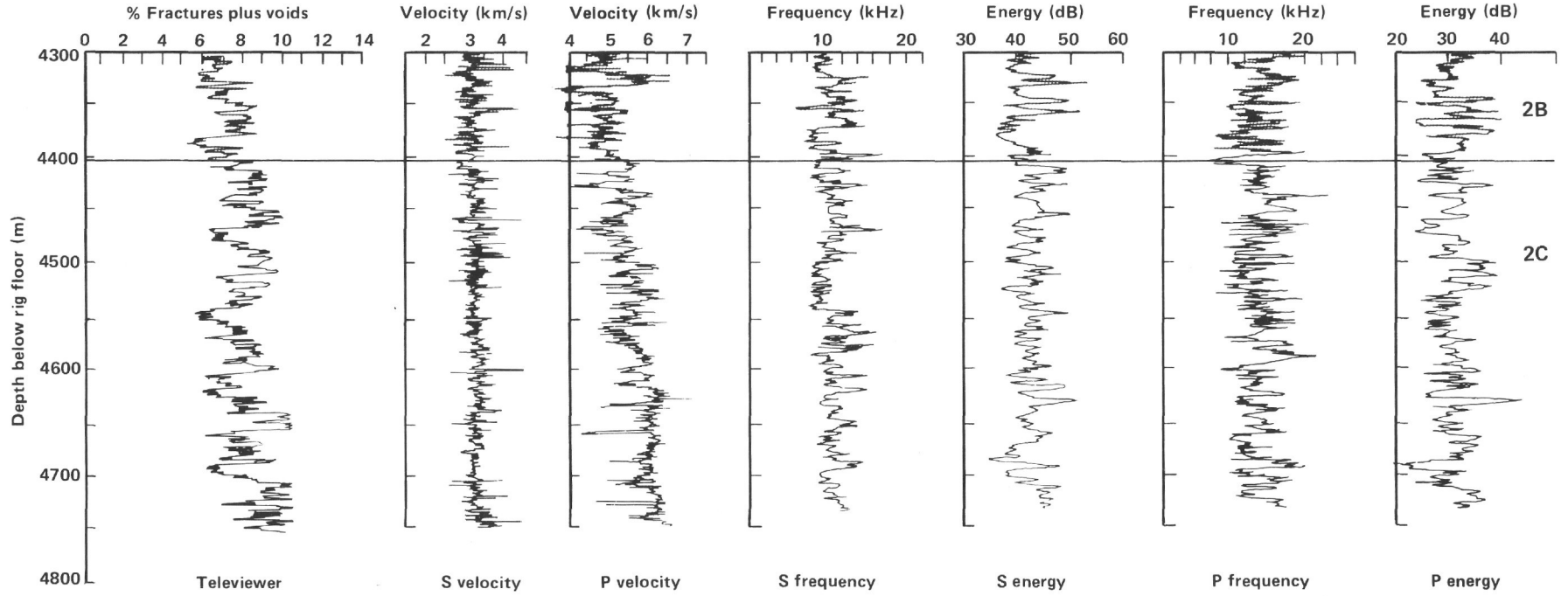


Figure 10. Fracture spectrum logs: P-wave and S-wave velocities, caliper, and BHTV fracture and void count from Figure 4 for Hole 504B, and energy and frequency of P-wave and S-wave coda from Figure 9 are shown in the dikes and transitional basalts at the top of the dikes (above line). Only in this area does the hole caliper show deviation from gauge.

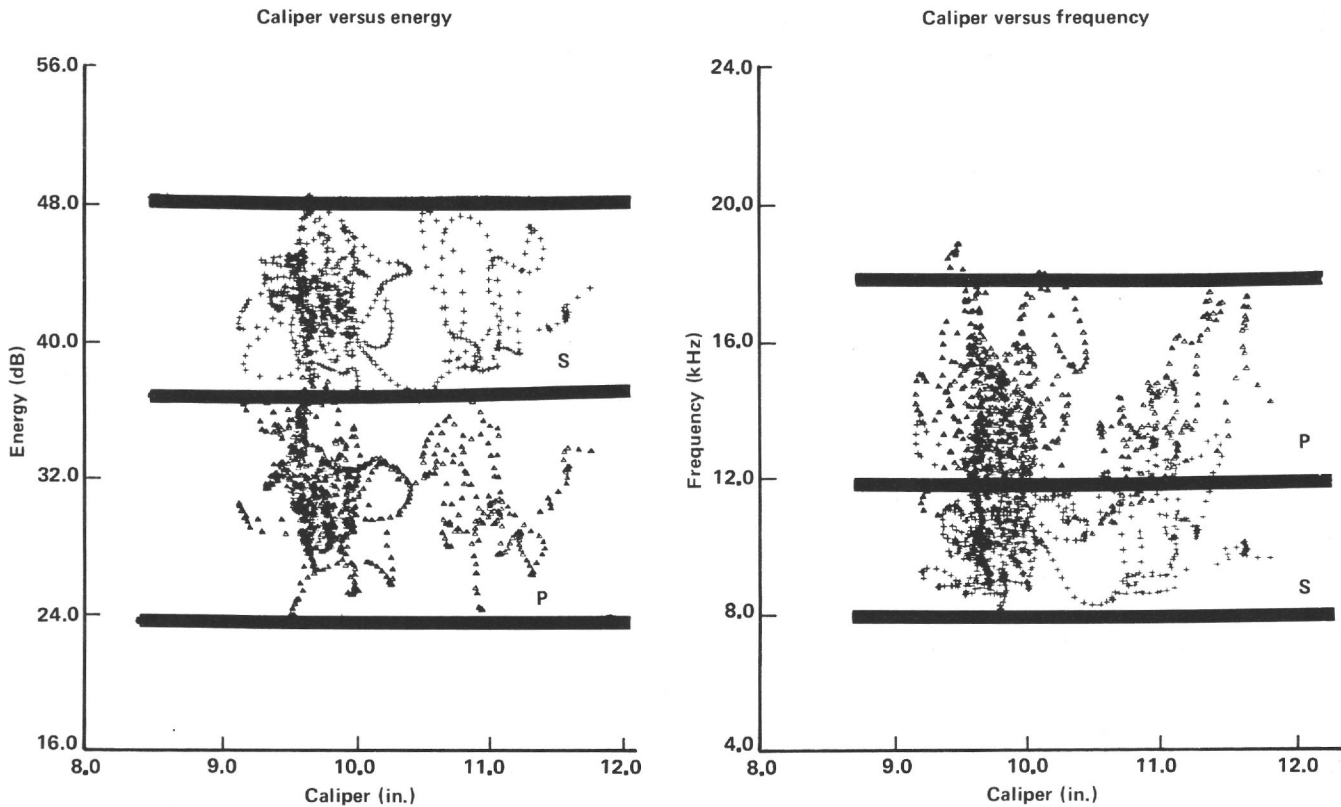


Figure 11. Caliper cross-plotted against compressional and shear coda energies and frequencies to demonstrate that there is no correlation in the dikes between borehole size changes and spectral changes.

(Fig. 13). The stronger correlation between energy and fractures than between energy and alteration extent implies that fracturing is the dominant process within which the spectra are changed in the dike section of the hole. Such might not be the case in the heavily altered Layer 2B pillow basalts, but we were not successful in deriving the cross spectra within this layer, as detailed previously.

Returning to the "fracture-spectrum" data presentation, we can make traditional log analysis cross-plots as well. (Fig. 14). We find rather surprising results. P energy is low when P frequency is high, as would be expected from low-pass filtering caused by scattering in fracture interfaces (Menke, 1983), but shear coda energy is low when S frequency is low, the opposite from that expected from scattering.

Shown another way, we find positive phase difference at the 60–70% level between shear frequency and energy, and 30–40% phase difference between compressional energy and frequency at about 7–70-m wavelengths (Fig. 15). The latter means that 60–70% of the time P energy is high when P frequency is low. Correspondingly, 60–70% of the time shear energy is high when shear frequency is high. These phase coherences, although only in the 60–70% correlation range, corroborate what our eye sees in the cross-plots (Fig. 15 versus Fig. 14).

This difference between the spectral responses of compressional- and shear-wave propagation becomes easier to explain if we transpose our energy-frequency spectra to energy-wavelength space. This wavelength is that of the sonic energy itself and, as such, is completely differ-

ent from the wavelength of phase difference up and down the hole discussed previously. Here, wavelength is calculated by dividing velocity by frequency at each measurement point. If we then display energy versus this sonic wavelength, we see a clear delineation of the spectral response we have observed in the dikes at the bottom of Hole 504B (Fig. 16). An *anti-resonance* or energy loss at characteristic wavelengths within the dikes is observed. Energy propagating at 30–40-cm wavelengths is being attenuated by the rock. Since we also observe a correlation of low-energy levels with zones of fracturing (Fig. 12), we can say that energy with these wavelengths is being lost into the fractures intersecting the well bore within these zones of intense fracturing. We can then discuss the length of fractures required to produce such a natural anti-resonance, if and only if we are certain that the anti-resonance is caused by geology and not by tool interference with the well bore or other geometric effects. Dimensions of fracturing carry information about permeability, both hydraulic and acoustic, since intersection of the well bore by fractures of a certain characteristic length might be required to produce a naturally occurring anti-resonance. How then can we eliminate the possibility that tool geometry is causing the observed loss of 30–40-cm wavelength energy? One way is to turn to another hole drilled into a different geology, but one logged by the same Schlumberger tools. If the same anti-resonance is found in that hole as in Hole 504B, then we are almost certainly looking at a tool-generated phenomenon; if, however, the filter characteristics at such a

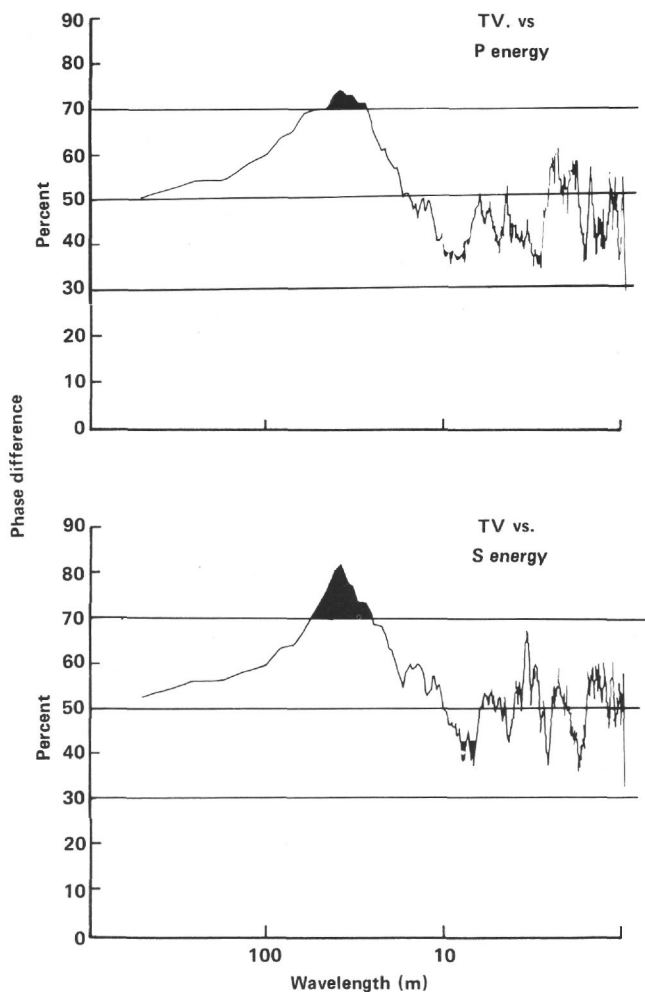


Figure 12. Phase difference of TV (BHTV fractures plus voids) and P and S energy in Hole 504B from Figure 10. Positive correlation is between high energy and zones of low fracture level.

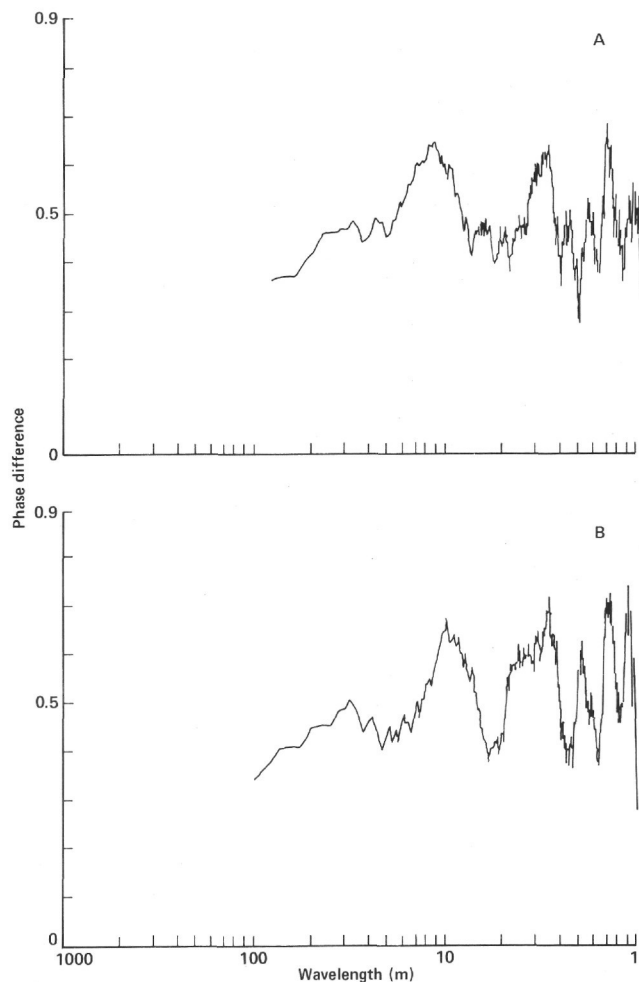


Figure 13. Phase difference between alteration content and (A) compressional, (B) shear coda energies over the dikes from 4300 to 4750 m into Hole 504B.

well are different from those in Hole 504B, then geology becomes the suspected cause of the anti-resonance.

GEOPHYSICAL LOGS FROM 17-Ma MID-ATLANTIC RIDGE CRUSTAL HOLE 556

Hole 556 from the Mid-Atlantic Ridge flank (Fig. 17) is the only other borehole with both significant penetration into the oceanic crust and a set of high-quality, Schlumberger geophysical logs comparable to those run in Hole 504B. (We also examined Holes 558 and 564 drilled on the same leg, but found the crustal section in each to be too short to generalize—65 and 50 m, respectively.) Yet the geological contrast provided by this well could not have been chosen better. First, exactly the same logging tools were used to log Hole 556 on Leg 82 as were used at Hole 504B on Leg 83 two months later. Second, the same model and gauge of drill bit was used. Third, an entirely different basement lithology sequence was penetrated in the 177.5 m of oceanic crust drilled at Hole 556.

Beneath 461.5 m of mostly carbonate sediments, a complex lithology sequence was encountered. First, 10 m of basalt breccia and intermixed carbonate sediment

were encountered, then 35 m of pillow basalts overlay a massive basalt unit and 40 m of basaltic breccia. For the first time significant thicknesses of gabbro and serpentinized gabbro were penetrated. Interlayered gabbro, gabbroic breccia, and serpentinized gabbro extended from 90 m sub-basement to the total depth of 177.5 m into the crust. Obviously, the gabbros are more characteristic of Layer 3 rocks and should not have been encountered so close to the surface. Their occurrence allows us to contrast tool responses in differing metamorphic lithologies within Hole 556 as well as with Hole 504B.

Geophysical Logging In Variable Metamorphic Lithologies

The variable lithologies identified previously were from identification of core, recovery of which dropped from close to 50% in the basalts to less than 20% in the gabbros (Bougault, Cande, et al., in press). They were located stratigraphically from major changes in geophysical log characteristics at the approximate depths within which the cores were taken (Hill and Cande, 1983). We wish to examine in detail these log changes. But we must understand tool responses to the different lithologies if

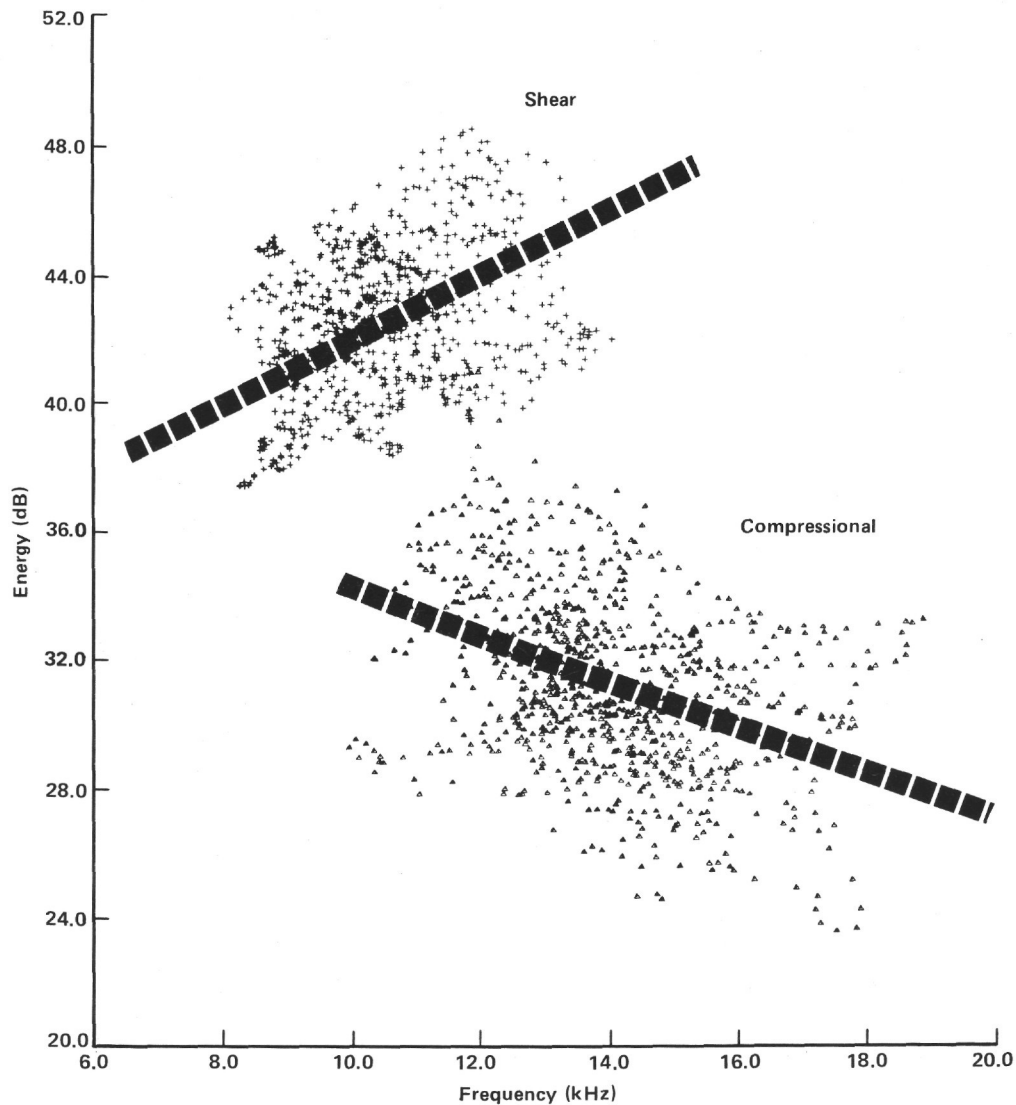


Figure 14. Both compressional (+) and shear (Δ) energy cross-plotted against frequency from Figure 10 for Hole 504B. While the data scatter considerably, trends indicated by the heavy dashed lines are evident.

we are to compare logging results with those in Hole 504B.

Porosities calculated from the neutron, gamma-ray, resistivity, and sonic logs in the standard way are displayed with raw resistivity, density, natural gamma-ray, compressional and shear velocity, Poisson's ratio, and caliper logs in Figure 18. Major lithology boundaries are evident from the density log, the resistivity log, and the differences between the various porosity logs at each depth (Fig. 18). For example, the very bottom of the hole is a gabbroic breccia with relatively low density and only a small difference between neutron and gamma-ray porosities, whereas the serpentized gabbro just above has very high density, but also large differences between neutron and gamma-ray porosity.

The existence of variable alteration-lithologies in Hole 556 allows us to test our hydroxyl-mineral content differencing scheme with more sophisticated commercial cross-correlation shale index techniques. Specifically, five "clay content" curves were generated for Hole 556 using

CORBAN ANSWERS (mark of Schlumberger, Ltd.) (analyses by J. E. McDonald, Schlumberger Offshore, New Orleans). Their averaging scheme again selects the minimum of these five curves at each depth point down-hole (Fig. 19). The Corban interpretation (VCL) improperly identifies much of the bound water as free water porosity (ϕ) because of very low clay volumes calculated from the resistivity and natural gamma-ray logs. This points to the difficulty in using standard oil-field techniques for the very different scientific logging requirements of the oceanic crust.

Our neutron-gamma-ray differencing scheme gives hydroxyl contents very similar to the neutron-density cross-plot values calculated by Corban (Fig. 19, far right for ours versus far left). The two serpentized gabbro zones made up of over 60% hydrated minerals show up nicely on either our differencing scheme or the Corban N-D cross-plot curves. Both predict a marked increase in hydroxyl-mineral content from the gabbroic breccia to the serpentized gabbro units, as was verified by the chemi-

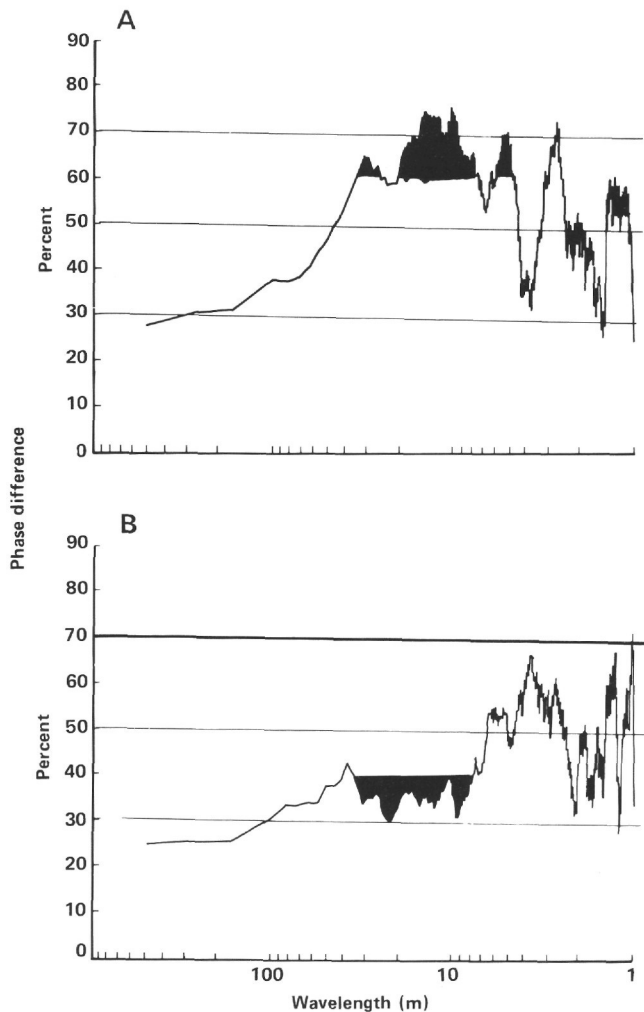


Figure 15. Phase difference analysis of the cross-plot shown in Figure 14 for Hole 504B, verifying a 60 to 70% correlation rate between high shear energy and high frequency (A) and a similar correlation rate between high compressional energy and low frequency (B). Wavelengths greater than 70 m are distorted by the ends of the log—that is, the log is not long enough for accurate phase difference calculations at these wavelengths.

cal bulk analyses of the cores (Bougault, Cande, et al., in press). We find that free water residing as porosity in the basement drilled in Hole 556 is small compared to the amount of water bound within hydroxyl minerals in the heavily altered gabbro and basaltic breccia sections of the hole.

An excellent lithology identification scheme seems to be an oil field technique called *M-N cross-plotting*. *M* and *N* are calculated as follows:

$$M = (\Delta t_f - \Delta t / \rho_b - \rho_f) \cdot 0.01$$

$$N = (\phi N_f - \phi N) / (\rho_b - \rho_f)$$

where

- Δt = travel time
- ρ_b = gamma-ray density
- ϕN = neutron porosity

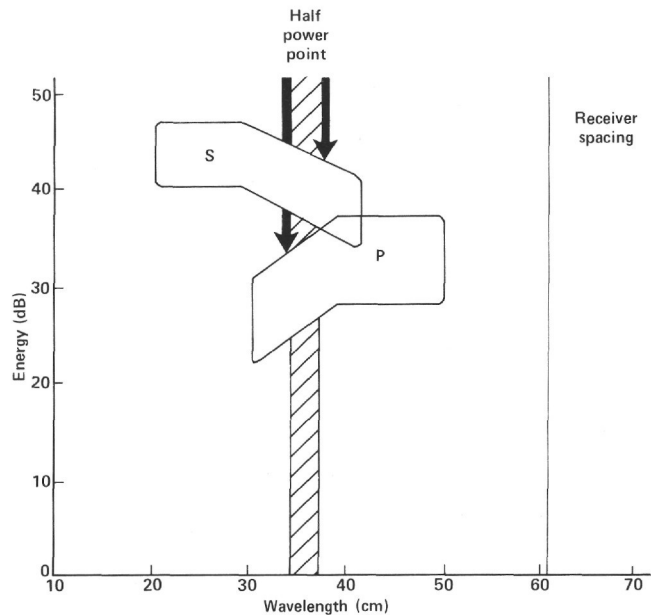


Figure 16. The energy-frequency cross-plot of Figure 14 can be transposed to an energy-wavelength cross-plot by calculating velocity divided by frequency at each data point. The data for Hole 504B then fall within the envelopes shown above. The half power point is the 3-dB down point of each data cluster. We interpret the energy drop at 30–40-cm wavelengths to be from anti-resonance.

$$\rho_f = \text{fluid density}$$

$$\Delta t_f = \text{travel time in borehole fluid}$$

Such a cross-plot identifies characteristic regions for each lithology. Serpentinized gabbro, for example, has *M* values ranging from 0.7 to 0.8 and *N* values of about 0.3; whereas gabbroic basalt has *M* of 0.8 and *N* of 0.5. Pillow basalts are closer to an *M* of 0.7 and an *N* of 0.45 (Fig. 20). We know these values in this well because cores were recovered, but lithologies of future wells could be determined solely by the *M-N* cross-plot once we have confidence in the lithology locations on the cross-plot. For example, some oil and gas is found in igneous reservoirs in Argentina, and, consequently, Schlumberger scientists have previously located the basalt and gabbro standardized points on the *M-N* cross-plot (Khatchikian, 1983). The oceanic crustal points are a little higher than these land points for both *M* and *N* (Fig. 20). An ultimate end to such a log calibration would be lithology identification without core being available.

Spectral Response of Hole 556 Oceanic Crust

Once we have identified lithologic units within the geophysical logs from Hole 556, we can return to our original problem: does anti-resonance exist in the sonic waveform spectra from Hole 556?

We are lucky that exactly the same multichannel sonic-logging tool was used in Hole 556 as in Hole 504B. We windowed the compressional- and shear-wave coda, did cross spectra, and displayed the energy and frequency in exactly the same manner as in Hole 504B (Fig. 21A,B). We then display the same frequency-energy cross-plot of compressional (Fig. 22A) and shear

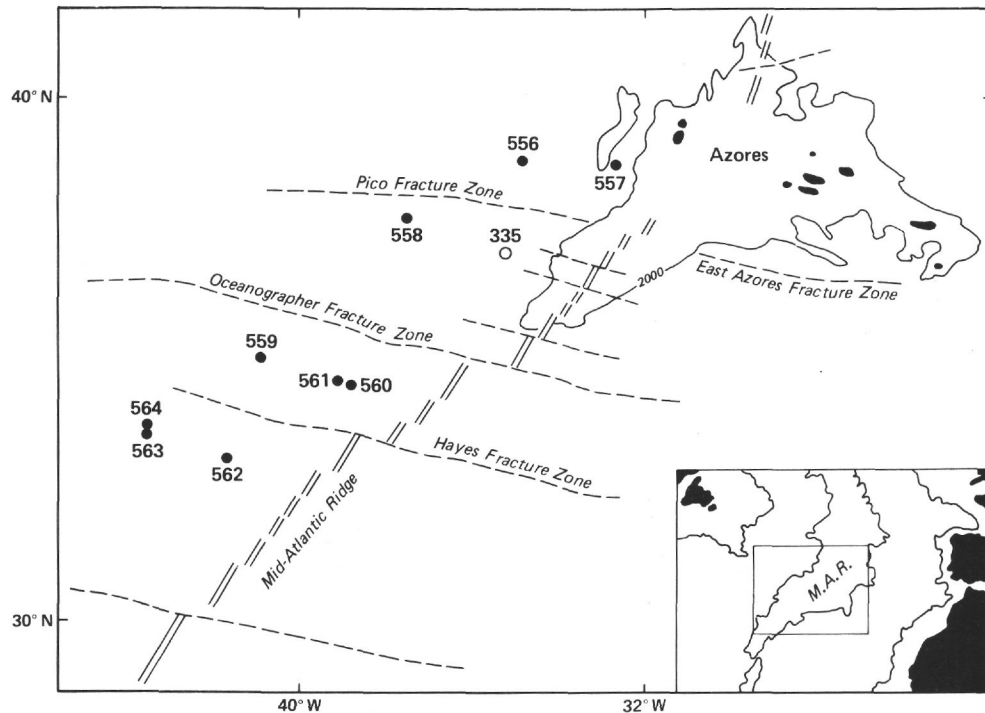


Figure 17. Location map for DSDP Hole 556 drilled at $38^{\circ}56.38'$ north latitude and $34^{\circ}41.12'$ west longitude in 3672 m water depth. Total penetration was 639 m, 461.5 m into calcareous sediments and 177.5 m into basalt and gabbro.

spectra (Fig. 22B). The attenuation of both the compressional-wave and shear-wave coda suggests passage of the energy through a medium acting as a frequency-dependent attenuator. In the case of compressional energy, this observation is opposite that from Hole 504B in that frequency is low when energy is low (Fig. 22A versus Fig. 14). No anti-resonance characteristic is evident in the waveform spectra from Hole 556.

In fact, alteration and lithology change can account for part of the "filter characteristics" observed in the spectra. If we observe spectral response to lithology changes, we find that the gabbros are high-energy, high-frequency formations that act as a high-pass filter (Fig. 21C). However, the serpentinized gabbros are low-energy and low-frequency rocks (Fig. 21C). For example, consider the bottom of the hole again. We can even identify a gabbroic breccia stringer within the serpentinized gabbro layer from a small energy and corresponding frequency increase at 10–15 m above total depth (Fig. 21B).

We can quantify the observation from Figure 21C of frequency-dependent attenuation by producing a log of compressional and shear coda center frequency and integrated energy as in Hole 504B (Fig. 23). Phase difference analyses, as before, reveal strong positive difference between compressional versus shear energy levels, and positive but weak coherences at wavelengths of 20–100 ft. between both compressional and shear frequency versus energy (Fig. 24). That is, there are zones of high- and low-energy level in the well that also appear filtered, in that high-energy zones are also high-frequency zones, and vice versa.

In this hole, we have no information on the distribution of fracturing within the different lithologies because

no BHTV runs were made. Fracturing might be expected to control the shorter wavelength phase differences because the crust appears to be so highly fractured.

We can examine, however, the relation between alteration and these long wavelength spectral changes in the hole. Phase difference between the hydroxyl-mineral content we calculated earlier and the spectra shows weak negative difference in the compressional and shear energies at long wavelengths (Fig. 24).

To demonstrate this correlation further, we detrend and bandpass filter the spectral and alteration content logs passing only energy with 20–100 ft. wavelengths (Fig. 25). We invert the bandpassed alteration log so that high hydroxyl content now correlates with low energy or frequency in the plots of Figure 25. We see that the compressional energy variations down the hole correlate well with the shear energy changes and, to a lesser degree, with the alteration log. Correlation is most striking in the gabbros of the lower half of the hole.

The extent to which the long wavelength components of the spectra correlate with degree of alteration can be further quantified by calculating a correlation coefficient for the bandpassed data. There is a -0.42 correlation between the bandpassed shear energy log and alteration content (Fig. 26). This is equivalent to a phase difference of 29% in Figure 24. Compressional energy does not correlate as well, with a coefficient of -0.32 , or 34% phase difference. However, most of the alteration change in Hole 556 occurs in the gabbros at the bottom of the well. If we correlate only the alteration and spectral changes in this portion of the hole, we calculate a correlation coefficient of -0.55 , equivalent to a phase difference of 22% for shear energy versus alteration and

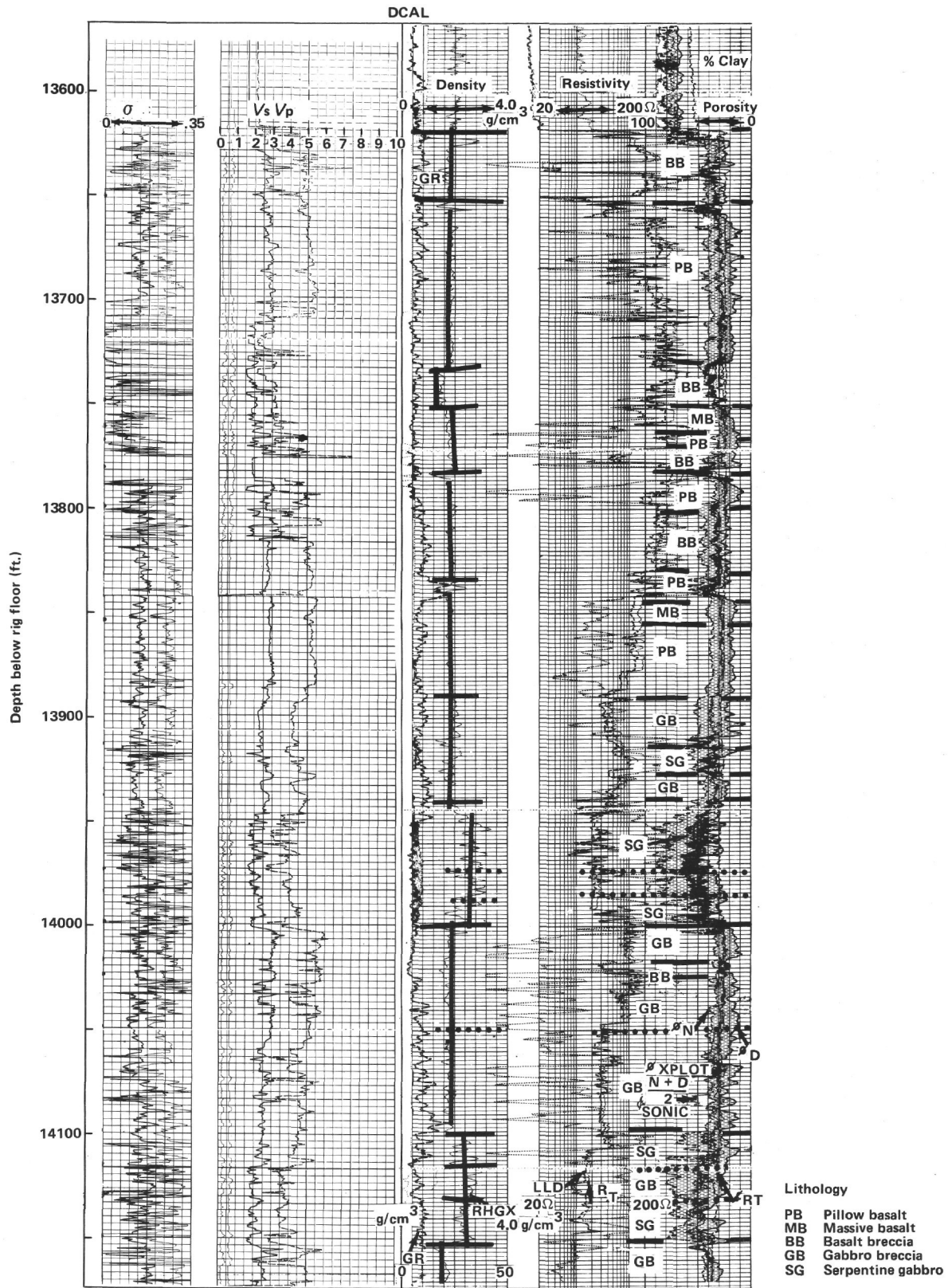


Figure 18. Composite logs run at Hole 556 by Schlumberger Well Services. *Center*: DCAL (caliper hole size minus bit size), gamma-ray density, and laterolog electrical resistivity. *Right*: several porosity determinations. Lithology boundaries were generally placed by the core recovery that decreased from about 50% in the basalts to less than 20% in the gabbros. Specific lithology boundaries were then determined from the changes in the porosity-sensitive logs. Several stringers are inferred where no core was recovered. Environmental corrections were for hole size, temperature, and pressure. Porosities are not corrected for bound water. *Left*: compressional and shear-wave velocity with Poisson's ratio as bold line on far left.

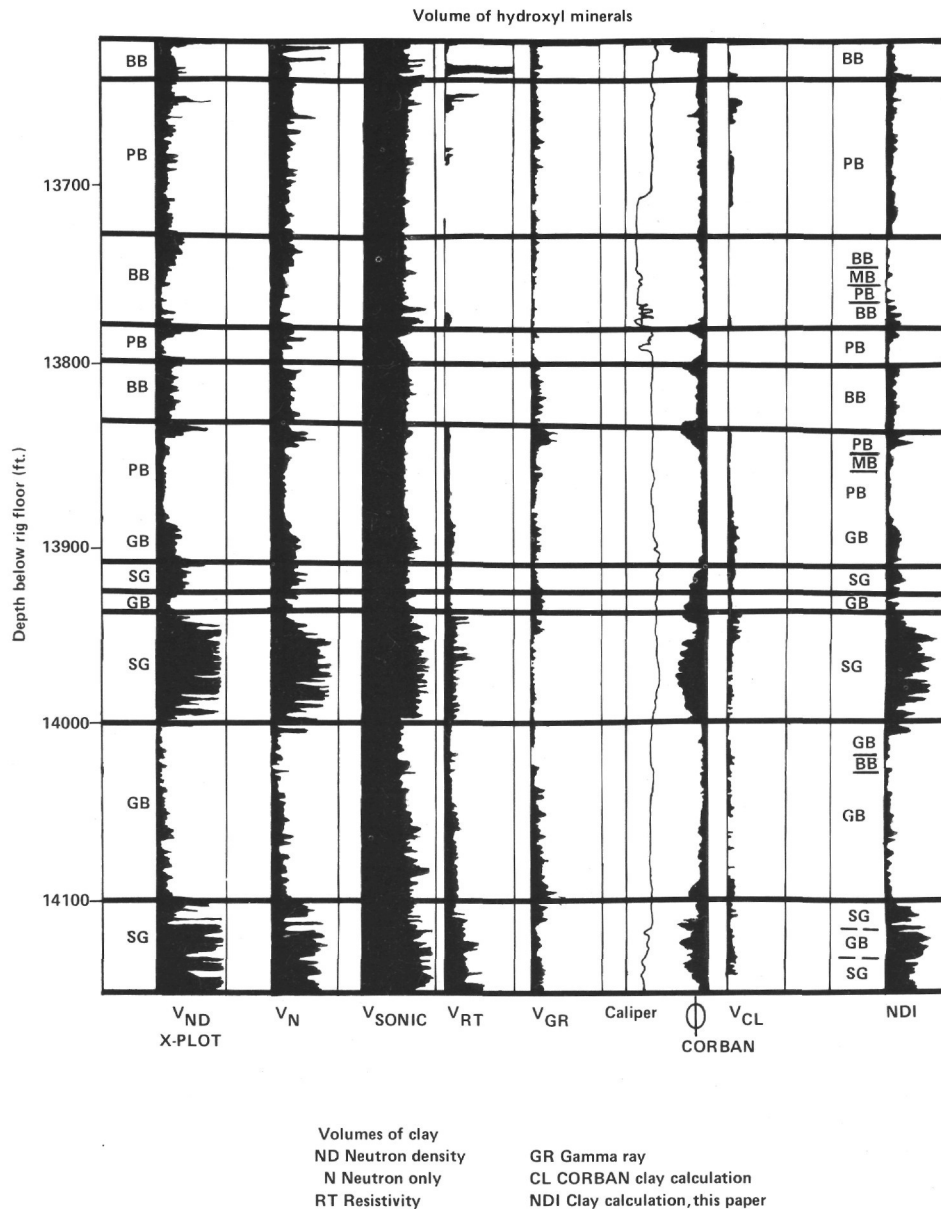


Figure 19. Clay-content log for Hole 556 as in Figure 3. Free water porosities for this hole are probably low, but the ratio is correct. Alteration has bound more water in hydroxyl minerals than is free in pore spaces in this hole. Fully 60% of the minerals in the serpentinite zones are hydrated. Clay-content log shown at right against CORBAN ANSWERS volumes of clay on left. Lithology boundaries as in Figure 18.

-0.45, or 28% for compressional energy/alteration (Fig. 26).

These weak correlations are to be expected since impedance changes that control the overall spectral response of the formation are caused by more than just alteration changes. We can examine some of these other effects qualitatively if we consider the formulation of impedance in the crust.

IMPEDANCE OF THE OCEANIC CRUST

Impedance is the opposition to the flow of energy occurring in a sound-conducting medium. The impedance changes caused by variable alteration lithology might give important insight into spectral changes occurring in the

oceanic crust. The sonic spectra respond in a very complex way to the impedance changes that occur downhole in the crust. We have isolated different responses from two holes in very different geology. In the Atlantic Hole 556, alteration and lithology changes resulted in frequency-dependent attenuation. In the Pacific, the lithology within the sheeted dikes of Layer 2C is absolutely constant. Yet, there the degree of fracturing varies down the hole. Anti-resonance must be a suspected result of some process occurring within this fracture system.

In fact, the impedance of the oceanic crust is too complex a function of too many variables for us to make much further progress in deciphering quantitative impedance cause-and-effect relationships. But we can iso-

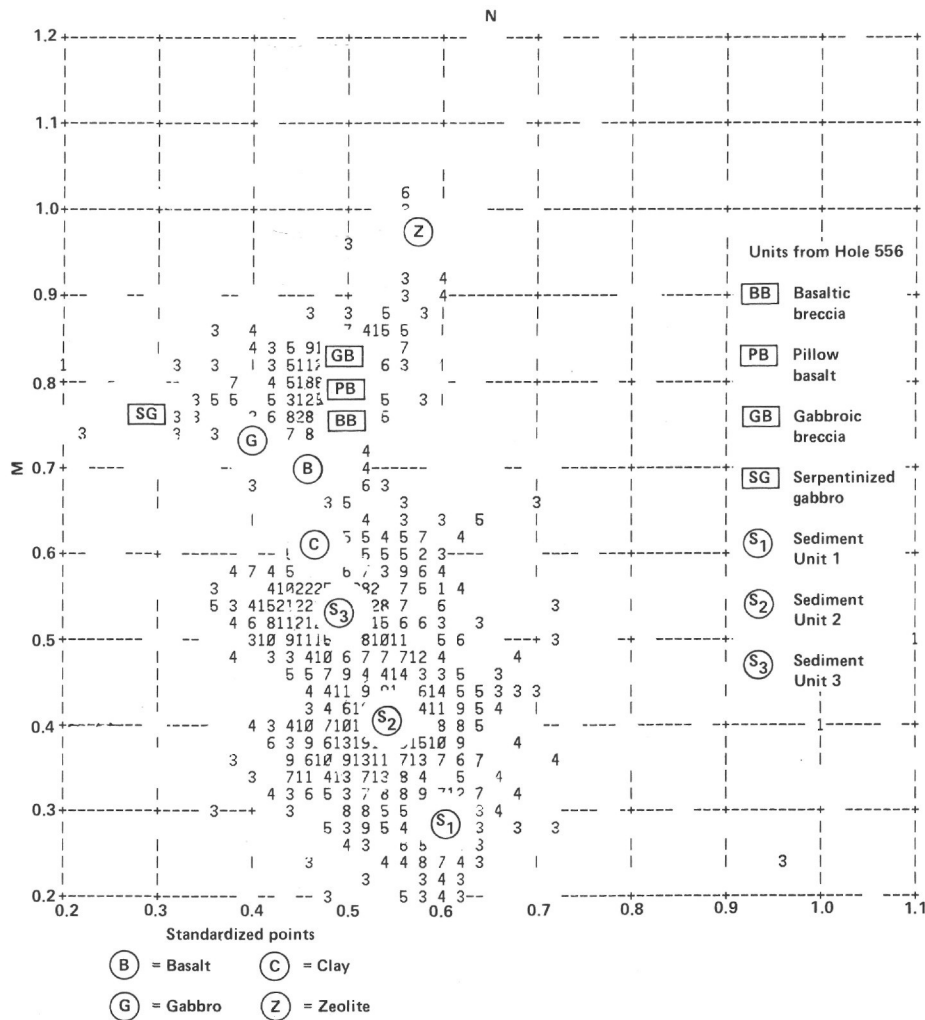


Figure 20. Lithologies are identifiable on an *M-N* cross-plot in Hole 556. S1, S2, and S3 are different sedimentary units. The igneous lithology locations other than those from Hole 556 are from oil-bearing formations in Argentina (Khatchikian, 1983).

late two factors that clearly are important for future logging and spectral studies of the oceanic crust.

First, we can define the impedance (*Z*) of the borehole rock system as:

$$Z = (\rho V^2 + 2\pi f t \rho - k/2\pi f t)^{1/2} \quad (3)$$

where

ρ = density in our case; mass in general, which equals the density measured by the logging tool because the volume sensed by the tool is constant

V = velocity,

f = frequency,

t = time, and

k = spring constant.

It is evident from this equation that direct observations of sonic velocity and rock density from geophysical logging do not provide enough information to constrain the impedance variations of the crust. Specifi-

cally, there are real (resistance) and imaginary (reactance) components to the impedance. Only the imaginary reactance terms are frequency dependent; the resistive real term generally has no frequency dependence. In Hole 556, we have observed variations in the power spectra of compressional and shear coda that appear to be dependent on alteration and lithology. Although frequency-dependent impedance changes are suggested, we do not have enough information yet to determine cause and effect. For example, there are two forms of imaginary reactance—mass reactance, which is equivalent to electrical inductance, and compliant reactance, which is analogous to capacitance. As frequency increases, mass reactance, which is density dependent, increases; and, as frequency increases, compliant reactance, which is dependent on the spring constant of the medium, decreases. We cannot determine yet which physical parameters in the crust of Hole 556 are affecting which reactance term. Other alternatives such as frequency-dependent coupling, scattering, or geometrical effects are also possible. We look forward to when we might be able to describe the transfer function of the oceanic crust.

We can speculate that part of the alteration effect on impedance within the crust in Hole 556 must be from the complex mass reactance term in Equation (3). For example, serpentinized gabbro must have higher mass reactance than gabbro because of its higher density (Fig. 18). Yet its high degree of alteration has also lowered its Poisson's ratio, which has some relation to the spring constant of the formation affecting the compliant reactance term. Somehow within Equation (3), serpentinized gabbro must offer less opposition to the flow of low-frequency energy, but more opposition to the flow of high-frequency energy to account for the observed changes in the spectra.

However, the absolute level of energy passing through the system is also affected. Recall that the spectra for the serpentinized gabbro zones exhibit low energy as well as low frequency (Fig. 21C). This overall drop in energy level may be a result of the real resistance increase caused by the higher density of serpentinized gabbro, although the velocity of both is less than that in the basalt zones (Fig. 18).

In addition to lithology, we can identify other major observational components to impedance changes in the oceanic crust (Fig. 26). Alteration changes within any of the crustal lithologies will certainly affect impedance. We have not been successful in isolating spectral changes that are due solely to alteration, though the use of a multichannel sonic-logging tool in the highly fractured Layers 2A and 2B in Hole 504B offers some promise. There the lithology is constant, and the degree of fracturing is severe in both layers, whereas alteration definitely increases from Layer 2A into Layer 2B.

Another variable that clearly affects impedance is mechanical—caliper size of the hole (Paillet, 1981). Zones of a poor hole have very different energy conversion characteristics than those at the boundary of a bit-sized hole. Our best policy with the study of the oceanic crust is to begin only in zones of good hole. Fortunately, with the exception of one serpentinite zone in Hole 556, both the dikes of Hole 504B and the rest of Hole 556 are gauge-sized holes (Fig. 18).

ANTI-RESONANCE AND VENTING IN THE SHEETED DIKES IN HOLE 504B

Whereas the spectra from Hole 556 appear to be affected by each of the major impedance changes in Figure 26, the waveforms from the dikes at the bottom of Hole 504B offer us a chance to isolate a single parameter. To be specific, caliper changes, lithology boundaries, alteration zones, and an unknown fracture pattern complicate the study of Hole 556 (no BHTV information exists at this site), but in Hole 504B, sheeted dikes have a gauge hole in a constant-lithology rock with little alteration present at the bottom of the hole (Figs. 2–4). The effects of fracturing on the acoustic impedance can be deciphered, at least to some degree. We are then interested in the implication of impedance changes for other physical properties of the crust such as permeability.

We can build a quantitative, though simplistic, acoustic model for the sheeted dike section of Hole 504B because fractures appear to dominate the impedance struc-

ture over this portion of the hole. Since we know the anti-resonance frequency within the system, we can calculate rather simply the length of fractures responsible for the anti-resonant behavior of compressional and shear waves in the dikes of Layer 2C in Hole 504B. Though this is an admitted gross oversimplification of the complex acoustic system operating in the crust, we can approximate the energy propagation in the dikes as occurring in interconnected tubes (fractures intersecting the borehole). The fractures then become a *half-wavelength* resonator.

Experimental and modeling results in air-filled tubes show that the effect of intersecting tubes is to vent energy from one tube into the other (Egolf et al., 1978). The effect on the energy spectrum is to create a resonance within the vent tube. Low-frequency energy is preferentially attenuated within such a vent system (Fig. 27). The vent tube length then controls the anti-resonance frequency within the half-wavelength resonator as well. That is, maximum energy loss within fractures intersecting the well bore will occur at the wavelength at which anti-resonance is set up within the intersecting fractures, which then vent energy away from the main energy propagation path. The frequency at which the first anti-resonance occurs is equal to the following:

$$f_a = (s + 1 - 1/2) (V/2L) \quad (4)$$

where

- f_a = frequency of the anti-resonance,
- s = harmonic number,
- V = velocity of sound, and
- L = length of the vent.

The half-wavelength resonator has resonances at whole numbered harmonics and anti-resonance in between. For shear waves in the dikes, f_a is 9 kHz, s equals 1 (the first harmonic), and the velocity is 3 km/s; the vent fracture length is 25 cm. We then suspect why the energy-wavelength cross-plot shows dramatic energy loss at 30–40-cm wavelengths (Fig. 16). Fractures intersecting the borehole appear to have a characteristic length of about 25 cm so that energy with wavelengths of 30–40 cm corresponds to the first anti-resonance within these fractures.

FILTER CHARACTERISTICS OF THE CRUST AND VENTING MODEL

Such a venting model makes specific predictions about the filter characteristics particularly applicable to the normal mode spectra. Specifically, the fluid waves should display high energy at high frequencies and low energy at low frequencies (Fig. 27).

The simplest quantitative analysis of the tube and fluid waveforms we can do is to FFT the entire wavetrain and display the power spectrum (color Fig. 28, appearing in frontispiece). Most of the compressional and shear coda energy is concentrated in a bandwidth of 10–25 kHz; the Stoneley energy is narrow band and centered at about 8 kHz (the highest amplitude, blue band at 8 kHz in Fig. 28). A source model with the Schlumberger sonic

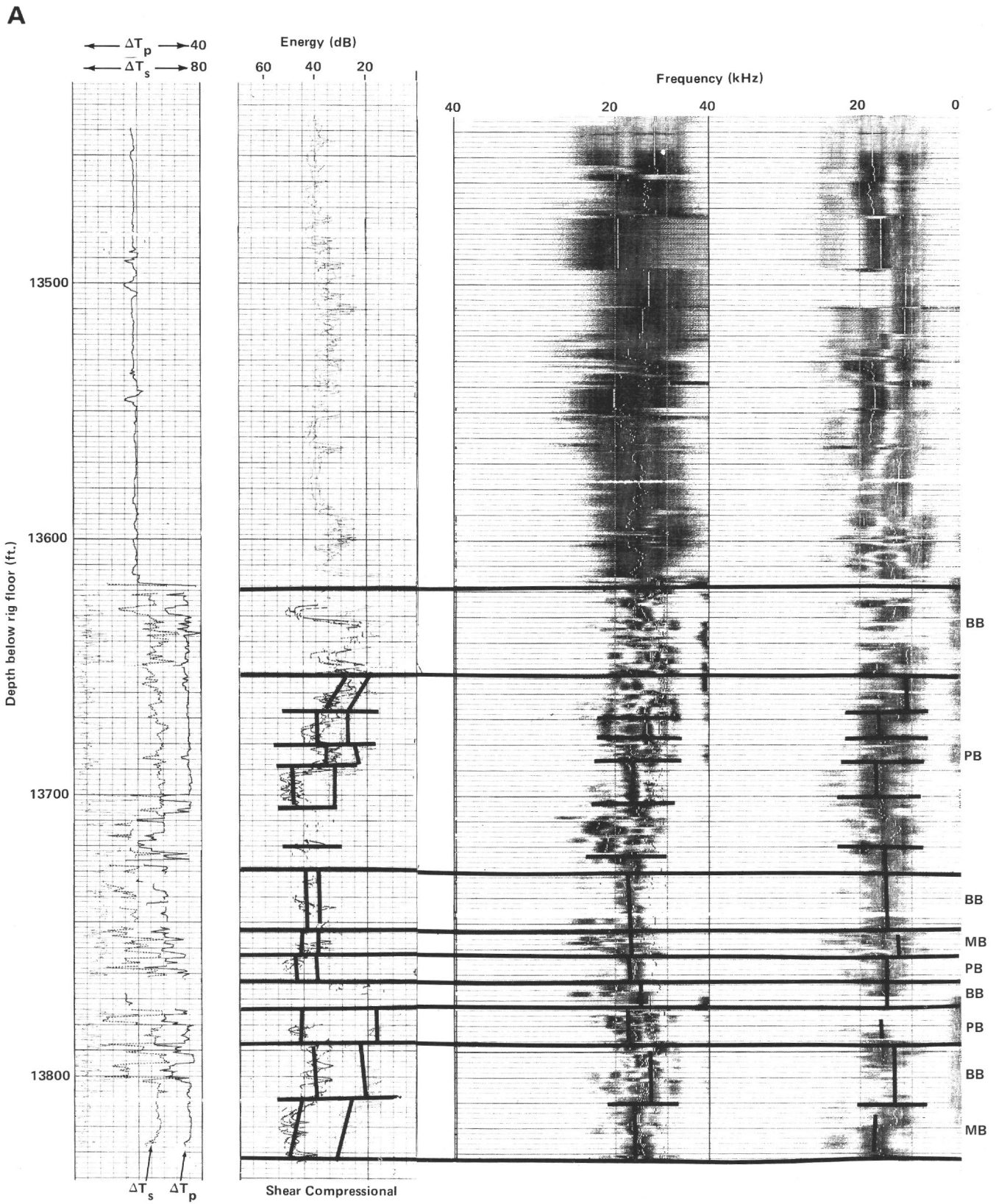


Figure 21. Energy-frequency cross spectra for Hole 556 as in Figures 8 and 9. Lithology units from Figures 18–20. The correlation between high energy and high center frequency and between low energy and low center frequency is clearly related to lithology. Figure 21C is a stylized schematic of the power spectra for compressional and shear energy in the four main lithology units of Hole 556 basement.

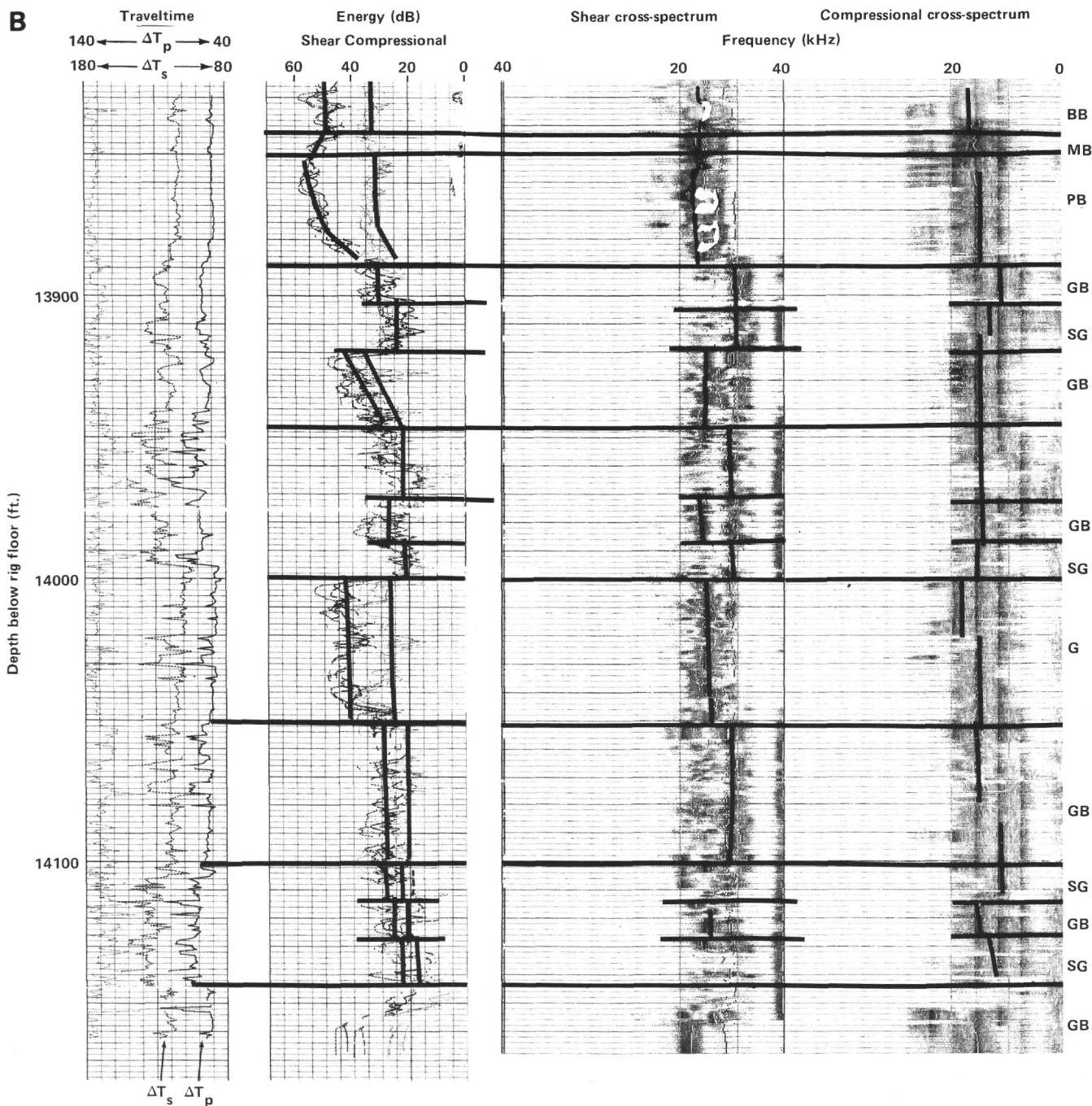


Figure 21. (Continued).

tool in a uniform cylindrical borehole predicts spectra for the normal modes that show a low frequency cut-off at 6 kHz for the first mode, 12 kHz for the second, and 24 kHz for the third (Fig. 29). Therefore, the predominant energy variation observed at 30–40 kHz (Fig. 28) is from these late-arriving normal modes. (Yellows are zones of high-frequency normal modal energy loss.)

These energy-level changes in the high-frequency normal modes can be qualitatively correlated with the pres-

ence or absence of fractures seen by the BHTV. For example, consider the zone of attenuation at 4715 m, which correlates with a fracture zone seen on the BHTV records (Fig. 28).

We can more quantitatively examine the possible filter effects of fractures on the Stoneley and normal modal spectra by placing a time window across these arrivals (Fig. 30). The window begins at a fixed time after source discharge set for a Stoneley velocity of 190 $\mu\text{s}/\text{ft}$. The

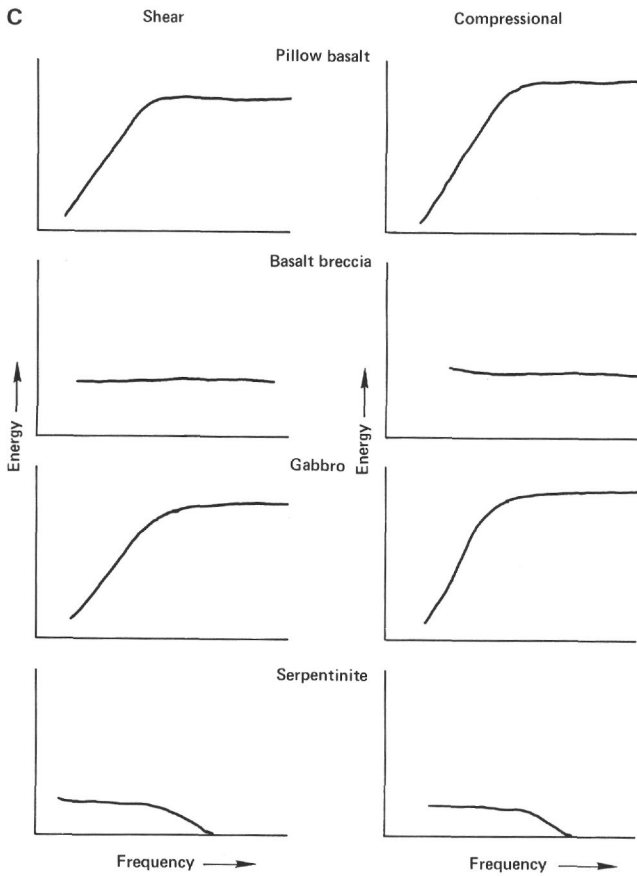


Figure 21. (Continued).

window has a duration of 450 μ s; also the frequency spectrum was low-pass filtered from 0 to 10 kHz with a linear ramp to 15 kHz to isolate the predominantly 8-kHz Stoneley energy.

Again concentrating on the dikes at the bottom of the hole, energy variations in the Stoneley energy correlate well with the variation in fracturing observed by the BHTV log (Fig. 31). Phase differences are the highest for any data pairs of this study, with a correlation of over 80%. These spectral changes are not caused by caliber changes as can be seen in Figure 31. These changes in the spectra clearly are not related to alteration changes, since no phase difference between alteration and normal mode energy exists at the bottom of the hole (Fig. 31).

But the Stoneley energy is not frequency dispersive (Fig. 29) and shows little, if any, change in frequency across fracture zones even though the energy level clearly drops. We have, therefore, plotted the peak energy and frequency of the normal modal coda within the same time window by excluding all energy below 10 kHz. These fluid wave arrivals are highly dispersive (Fig. 29) and should show a frequency decrease corresponding to energy attenuation in the zones of heavy fracturing if the venting model correctly predicts the filter characteristics of the dikes.

The peak frequency of the normal modes varies as predicted by the venting model (Fig. 32). When the energy level is high, the peak frequency is high; when the energy level is low, the peak frequency is also low. The normal modal energy changes also correlate strongly with the Stoneley wave energy levels as would be expected.

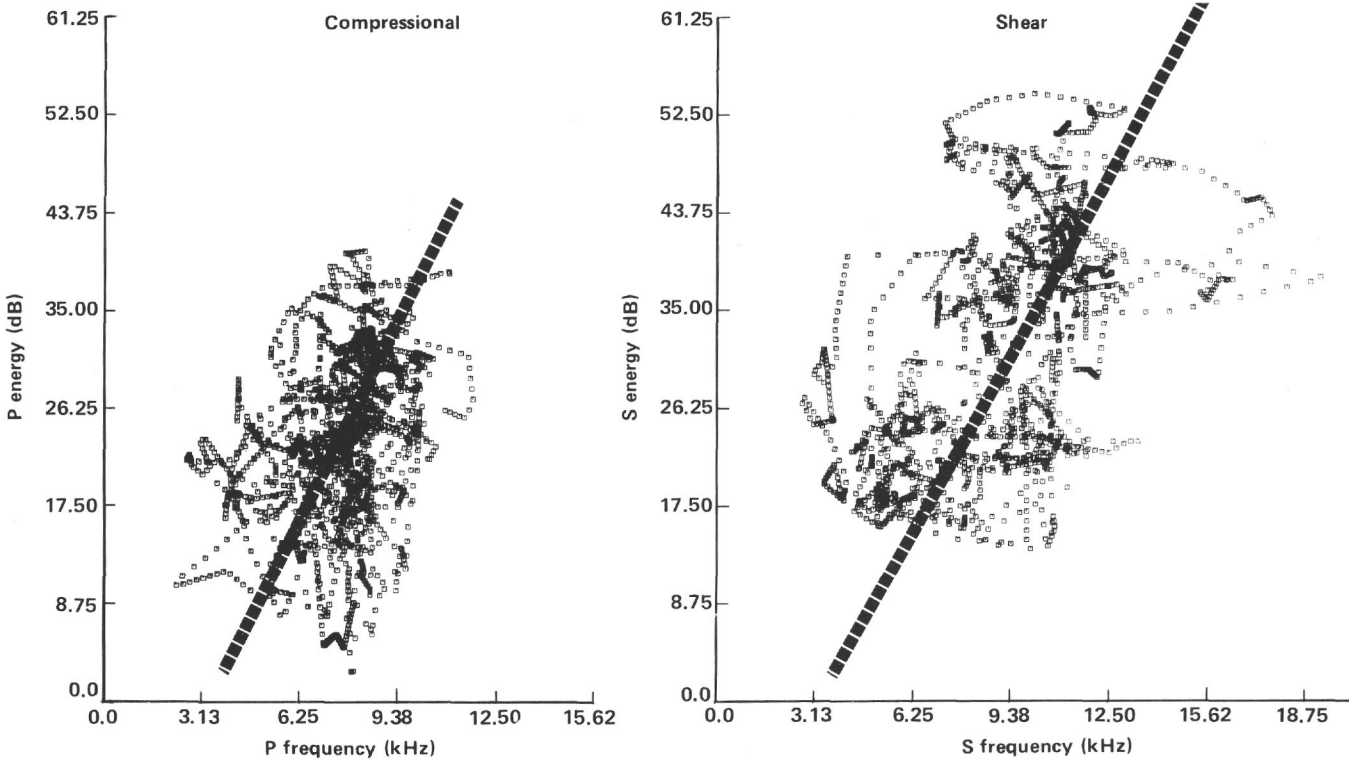


Figure 22. Energy-frequency cross-plots for compressional and shear coda from Figure 21 for Hole 556. While the data are scattered, the bold dashed lines indicate the trends apparent in the data.

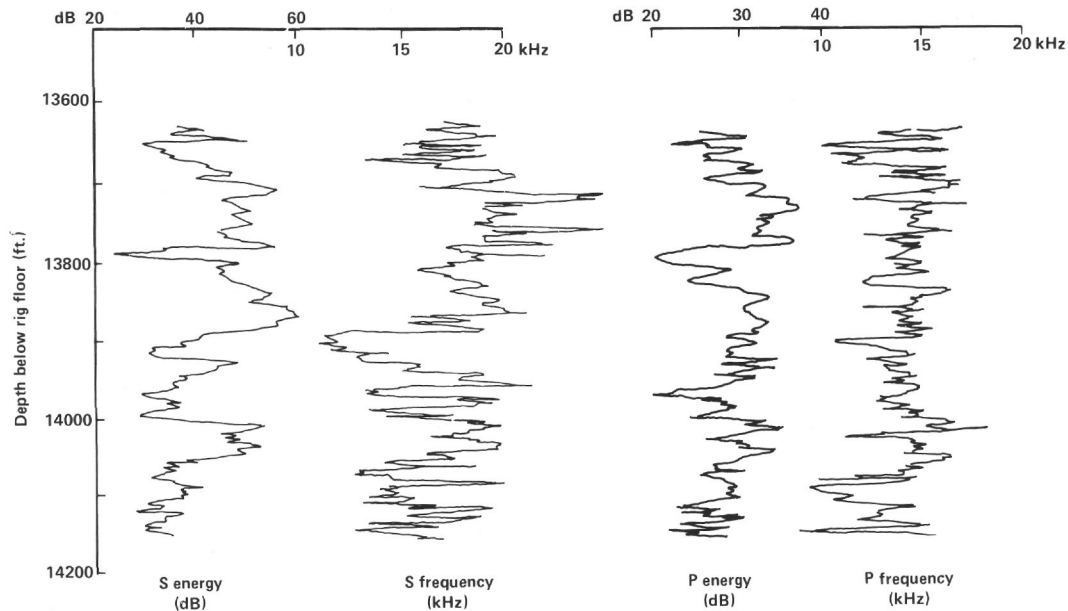


Figure 23. Spectrum log of compressional and shear coda energies and center frequencies for Hole 556 (as in Fig. 10).

ed (Fig. 32). Best of all, the normal modal energy and frequency correlate strongly with the fracture pattern seen in the bottom of the hole. When the hole is only lightly fractured, the normal modal energy and frequency are high, but when the well is heavily fractured, the modal energy and frequency are low (Fig. 33).

These correlations can be seen by bandpass filtering the Stoneley energy and normal-mode-spectral and fracture logs to pass only energy with strong phase coherence (Fig. 34). It is interesting that this filter passes energy of 10–100-m wavelengths. Earlier we thought that fracturing would produce a shorter-wavelength filtering effect. The fracture pattern is clearly consistent at longer wavelengths within the dikes than previously thought. That fracturing is concentrated in zones having a long-wavelength component was also concluded from a different logging data analysis by Newmark et al., this volume. Zones of intense fracturing 15–25 m thick are separated by zones of relatively solid basalt of similar thicknesses in the dikes at the bottom of Hole 504B.

It is important to note that the Stoneley wave itself does not contribute much to these spectral changes. Although it is the predominant energy wave within the window, its frequency remains relatively constant in the test interval. The normal modes provide the major energy and frequency shifts shown in Figs. 28 and 31–34.

We can ask now what aspect ratio of fractures within the zones of fracturing would be predicted by the venting model to produce the filtering effect on the normal modes. To understand better the effects of varying the size of vent fractures, we have conducted a series of model experiments in air-filled main and vented tubes of the same diameter in a lightly dampened medium. The vent opening away from the intersection with the main tube was changed to present variable diameter vent constrictions (Fig. 35). The purpose of this experiment is to map the effects of fractures with very small vent diame-

ters relative to the main transmission path versus those with relatively large vent diameters. We hope this model represents adequately the case of variable constriction diameters for fractures that intersect the borehole in the oceanic crust.

The experiment consists of a constant-voltage, pure-tone source that is stepped upward in 48 frequency steps from 100 H to 4 kHz. The energy output at the end of a main tube is measured at each step for each of five vent constriction to main tube ratios. The five different vent constriction to main tube ratios ranged from 0.17:1 to 1.06:1.

We discover that the effect of increasing the width of the vent constriction relative to the main fracture diameter is to shift the resonant frequency to higher frequencies and to increase the overall resonance and anti-resonance of the system (Fig. 35). Peak frequency drops as the overall energy level drops in the manner observed. The borehole vent model analogy would require, however, that zones of intense fracturing be composed of many, many more small-diameter fractures than zones of little fracturing, which must have a few relatively large diameter fractures. Then the spectral shifts seen in Figures 32 and 33 would match those observed in Figure 35.

In the oceanic crust, we expect to encounter a variably fractured medium so that constriction ratios of intersecting fractures would be highly variable. It is not surprising then that the large scatter in Figure 14 might result from the proposed venting mechanism if it is applicable to the oceanic crust. Maximum anti-resonance occurs, however, when the fractures are all about the same diameter.

We have not provided any direct proof that venting occurs in the oceanic crust. Instead, we have shown that a reasonable occurrence in a highly fractured rock of intersecting vents would provide the proper boundary conditions for the anti-resonance effects observed in the

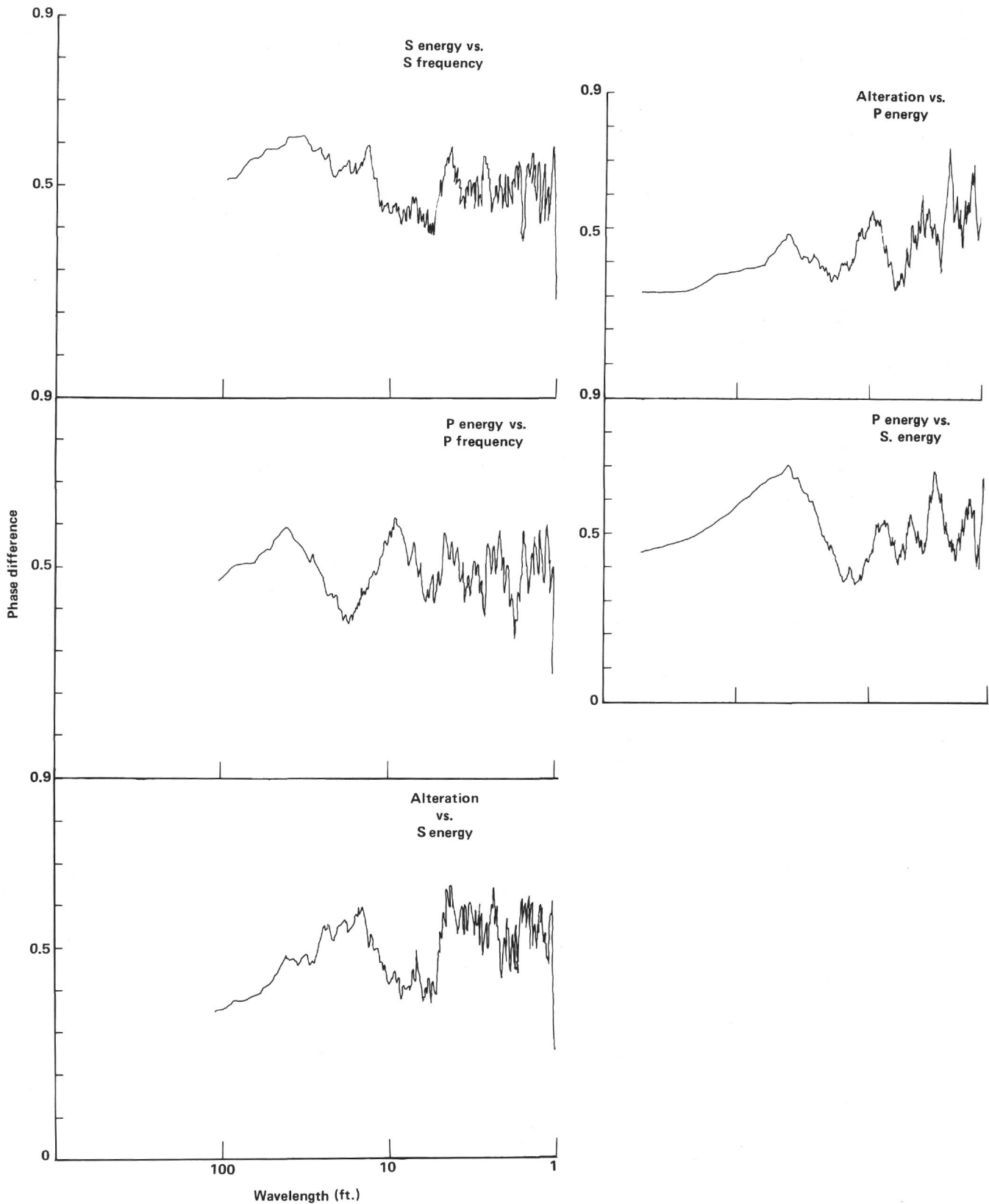


Figure 24. Phase difference between shear energy and frequency, and compressional energy and frequency for Hole 556 (as in Fig. 15). Phase difference between P and S energy and alteration content from Figure 19 displays slight negative correlation at long wavelengths.

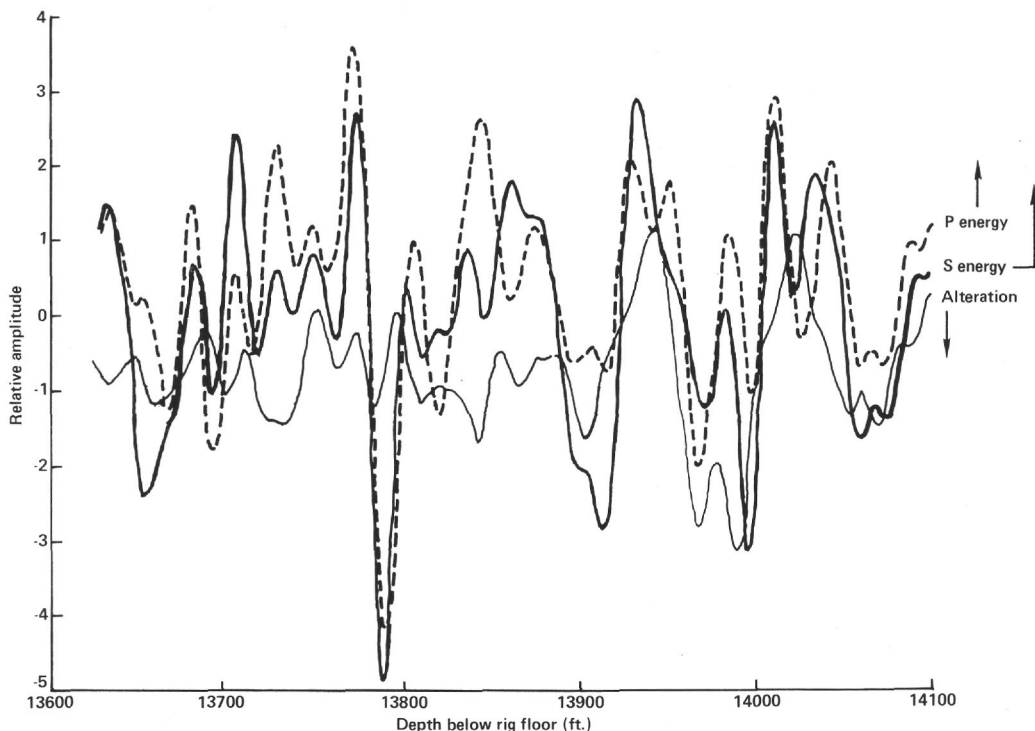


Figure 25. The P energy, S energy, and alteration logs from Hole 556 were then detrended, normalized, and band-pass filtered to pass only wavelengths of 20–100 ft. Note particularly strong correlation between P and S energy. Arrows indicate direction of increasing values of each curve.

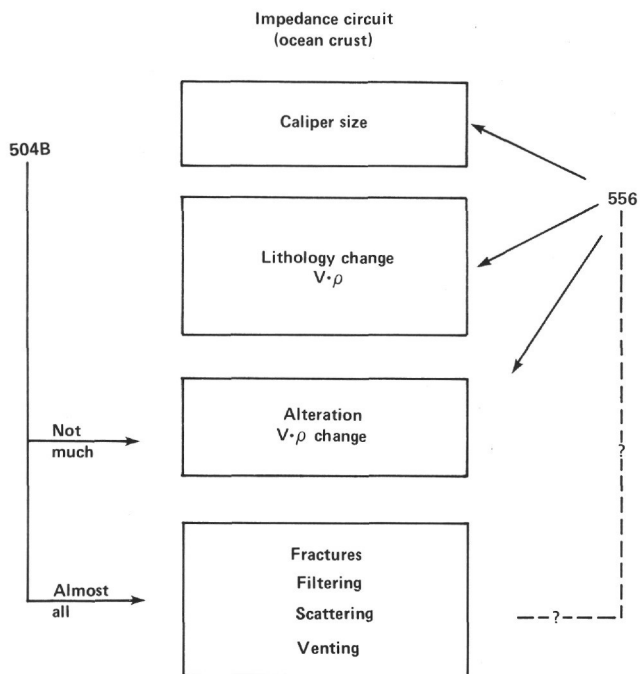


Figure 26. Schematic box diagram of the physical properties that affect formation impedance, and how the amount of information we have about Hole 504B compares with that of Hole 556.

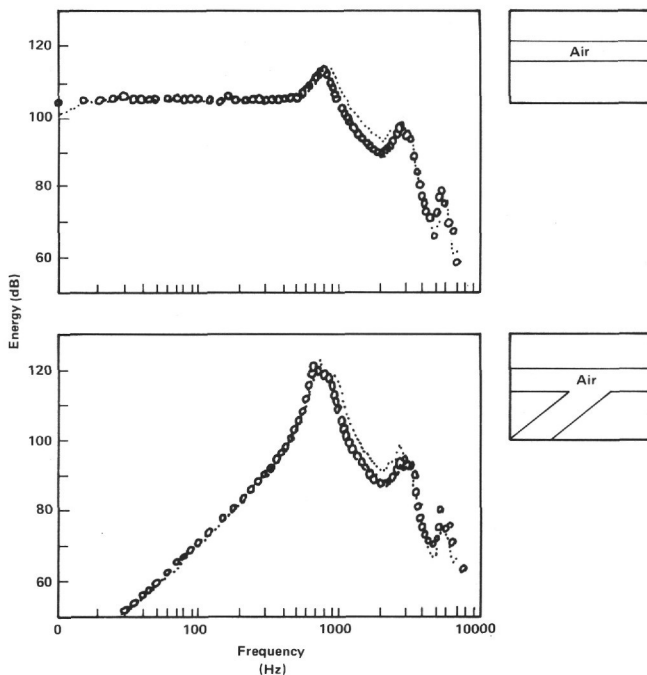
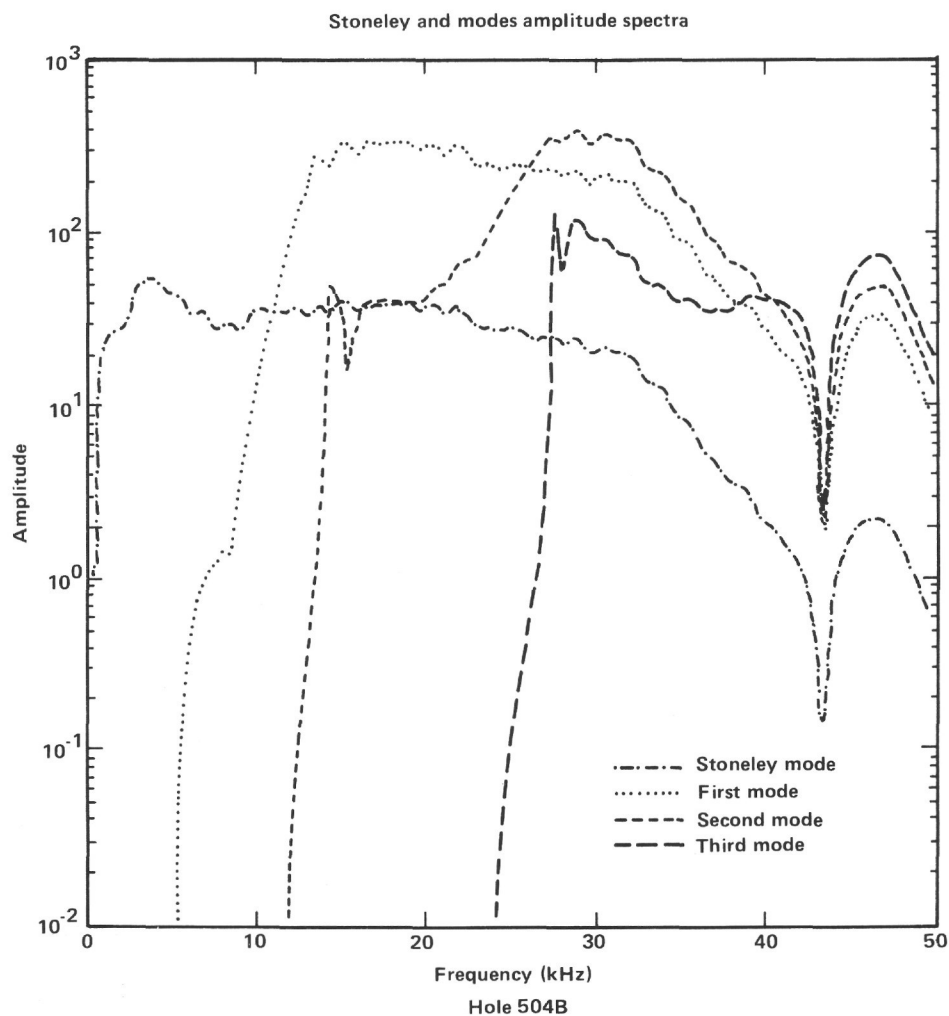


Figure 27. Change in the power spectrum for transmission of sound in an air-filled tube (top) versus the same tube with a vent intersecting it (from Egolf et al., 1978). The energy peak is caused by resonance set up in the vent. Open circles are observations, light dashed is prediction from a venting model.



Hole 504B

Layer	DTC (μ s/ft.)	DTS (μ s/ft.)	DEN	Radius (in.)	Q (COMP)	Q (SHR)
Tool				1.81		
Fluid	186.0		1.00	4.67	10000	
Solid	50.0	100.0	2.85	4.67	10000	10000

Model by Olive Liu, Schlumberger, Ltd., Houston.

Figure 29. Tool response model for upper transmitter of the Schlumberger SLS-5 sonic-logging sonde in a uniform cylinder. Note that Stoneley energy is nondispersive whereas normal modal energy is highly dispersive.

sonic waveform spectra within the dikes of Layer 2C in Hole 504B. Also, the Stoneley and normal mode filter characteristics of the dikes might be explained by the venting hypothesis. This venting effect is well known in acoustics and must be occurring to some degree in the highly fractured oceanic crust.

Assembling the anti-resonance, venting, phase difference, and bandpass filtering analyses into a final conclusion from this study, we find that zones of intense fracturing are periodic down the well. The dikes appear to be jointed into 15–25-m-thick zones of intense fracturing. Such zones are characterized by the occurrence of subhorizontal, but relatively small diameter fractures with average lengths of about 25 cm, separated every 15–25 m by zones of more solid basalt with fewer but larger-diameter fractures. We reach these conclusions from

the cross-correlation of the geophysical logs with the spectral changes seen in the sonic waveform logs. We predict that similar structures should be observable in the sheeted dikes of ophiolite complexes on land.

SUMMARY: EFFECTS OF PERMEABILITY CHANGES ON THE IMPEDANCE OF THE OCEANIC CRUST

We have shown that impedance changes are complex and difficult to quantify in the oceanic crust. These changes most certainly come about as a result of physical-property changes in the oceanic crust, yet specifying cause and effect will require more boreholes with more sophisticated logging than are presently available.

As an example of the importance of fully describing the impedance transfer function of the crust, consider

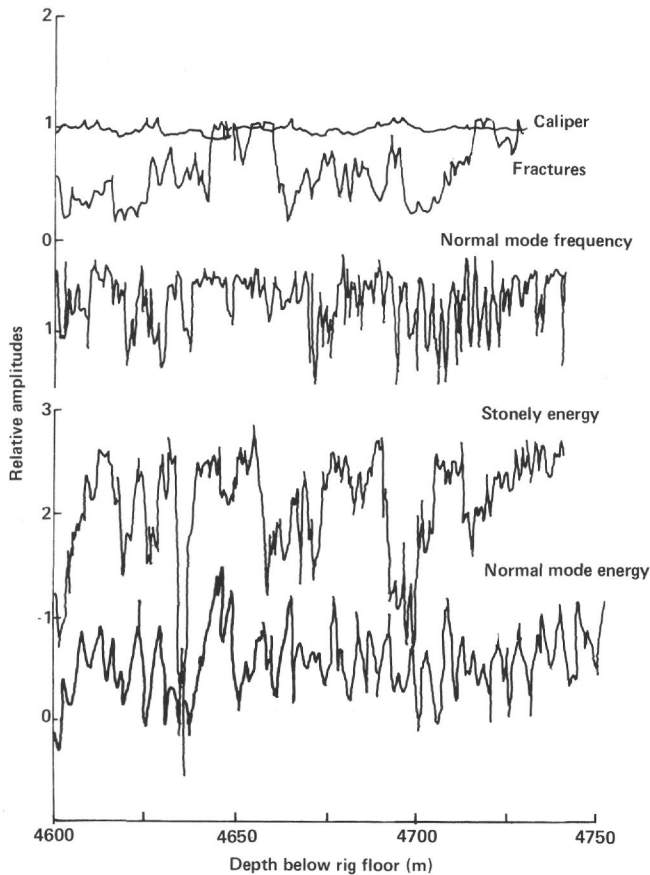


Figure 30. The fracture log over the lower 150 m of Hole 504B is displayed along with the amount of Stoneley wave and normal mode energy in decibels and peak frequency of the normal modal energy in kHz calculated from windowed sonic waveforms.

permeability. Fracturing and the degree to which alteration products fill those fractures control crustal permeability. Physical-property changes caused by the plugging of fractures with clay mineralization will produce impedance changes, which, though complex, are beginning to be understood. It appears likely that in the future we will be able to work backward from quantification of major impedance changes using geophysical logging to reconstruct the permeability history of the oceanic crust.

Hole 504B is a good locale to begin with because permeability has been measured over the entire section of crust by flow-test methods (Anderson and Zoback, 1983; Anderson et al., this volume). Because of excessive temperatures, however, a specific value could not be obtained in the sheeted dikes. Electrical resistivity measurements predict porosity changes that largely mirror the observed drop in measured permeability over Layers 2A and 2B (Fig. 36; Becker, this volume). If porosity changes from the electrical measurements are extrapolated into the dikes to guess at a value for the permeability for that layer, predictions are for very low values—near that of unfractured granite (10^{-20} m²) (Becker et al., 1983).

Although we could reach only simplistic conclusions about the spectral changes within the dikes, we can conclusively state that the dikes are at least “acoustically”

permeable. That is, energy (e.g., from normal modes) is being attenuated in zones of fracturing within the dikes. The fact that 30–40-cm wavelength headwave energy is also heavily attenuated within zones of fracturing in the dikes suggests that such zones are likely to be hydraulically permeable as well because intersecting vents are required if anti-resonances are to occur. We predict that the dikes are several orders of magnitude more permeable than unfractured granite, which would not attenuate and would have no vents.

In summary, geophysical logging in oceanic crust is only just entering an era where quantitative statements can be made about virtually every important physical property from *in situ* measurements made in deep boreholes. We have presented methods for the quantitative calculation of hydroxyl-mineral content of the formation; for the use of the BHTV fracture log and full waveform sonic log spectral changes to identify lithology, characterize fractures, and determine acoustic permeability, and for the use of integrated geophysical log cross-correlation to determine overall geology of Deep Sea Drilling Project holes. We look forward to the logging of many more crustal holes.

ACKNOWLEDGMENTS

We thank the officers, crews, and scientific parties of *Glomar Challenger* Legs 82 and 83, without whose diligence and hard work these logs could not have been successfully completed. Schlumberger, Ltd., kindly provided computer and analyst time for this project. We particularly wish to thank David Leslie and Olive Liu for performing the spectral processing used in this paper. They contributed invaluable scientific insight as well. Dan Moos, Dave Egolf, Keir Becker, Bill Murphy, Ken Winkler, and two anonymous reviewers greatly improved the content of this paper. None of this work could have been completed without the support and encouragement of Mark Zoback. This research was supported by Office of Naval Research Contract TO-0098, scope HH, and National Science Foundation Grant OCE 81-10919.

REFERENCES

- Anderson, R. N., Honnorez, J., Becker, K., Adamson, A. C., Alt, J. C., Emmermann, R., Kempner, P. D., Kinoshita, H., Laverne, C., Mottl, M. J., and Newmark, R. L., 1982. DSDP Hole 504B, the first reference section over 1 km through Layer 2 of the oceanic crust. *Nature*, 300:589–594.
- Anderson, R. N., and Zoback, M. D., 1983. Permeability, underpressures and convection in the oceanic crust near the Costa Rica Rift, Eastern Equatorial Pacific. *J. Geophys. Res.*, 87:2860.
- Becker, K., Langseth, M. G., Von Herzen, R. P., and Anderson, R. N., 1983. Deep crustal geothermal measurements, Hole 504B, Costa Rica Rift. *J. Geophys. Res.*, 88:3447.
- Becker, K., Von Herzen, R. P., Francis, T. J. G., Anderson, R. N., Honnorez, J., Adamson, A. C., Alt, J. C., Emmermann, R., Kempner, P. D., Kinoshita, H., Laverne, C., Mottl, M. J., and Newmark, R. L., 1982. *In situ* electrical resistivity and bulk porosity of the oceanic crust, Costa Rica Rift. *Nature*, 300:594–598.
- Bougault, H., Cande, S., et al., in press. *Init. Repts. DSDP*, 82: Washington (U.S. Govt. Printing Office).
- Egolf, D. P., Tree, D. R., and Feth, L. L., 1978. Mathematical predictions of electroacoustic frequency response of *in situ* hearing aids. *J. Acoust. Soc. Am.*, 63:264.
- Hill, I. A., and Cande, S., 1983. Downhole physical property measurements in Atlantic Ocean crust from wireline logging results. *EOS*, 64:314.
- Houtz, R., and Ewing, J., 1976. Upper crustal structure as a function of plate age. *J. Geophys. Res.*, 81:2490–2498.
- Khatchikian, A., 1983. Log evaluation of oil-bearing igneous rocks. *World Oil*, 79–82.

Menke, W., 1983. Frequency response from scattering of seismic energy by multilayered media. *Geophys. J. Roy. Astron. Soc.*
Moos, D., and Zoback, M. D., 1983. *In situ* studies of velocity in fractured crystalline rocks. *J. Geophys. Res.*, 80:2345.
Paillet, F. L., 1981. Predicting the frequency content of acoustic waves in boreholes. *22nd Ann. Logging Symp., Trans. Soc. Prof. Well Log Analysts*, Mexico City, p. 26.

Zoback, M. D., and Anderson, R. N., 1982. The implications of fracture distribution, structure, and stratigraphy from borehole televiewer imagery of the oceanic crust on the Costa Rica Rift, *Nature*, 295:375.

Date of Initial Receipt: 10 May 1983
Date of Acceptance: 15 February 1984

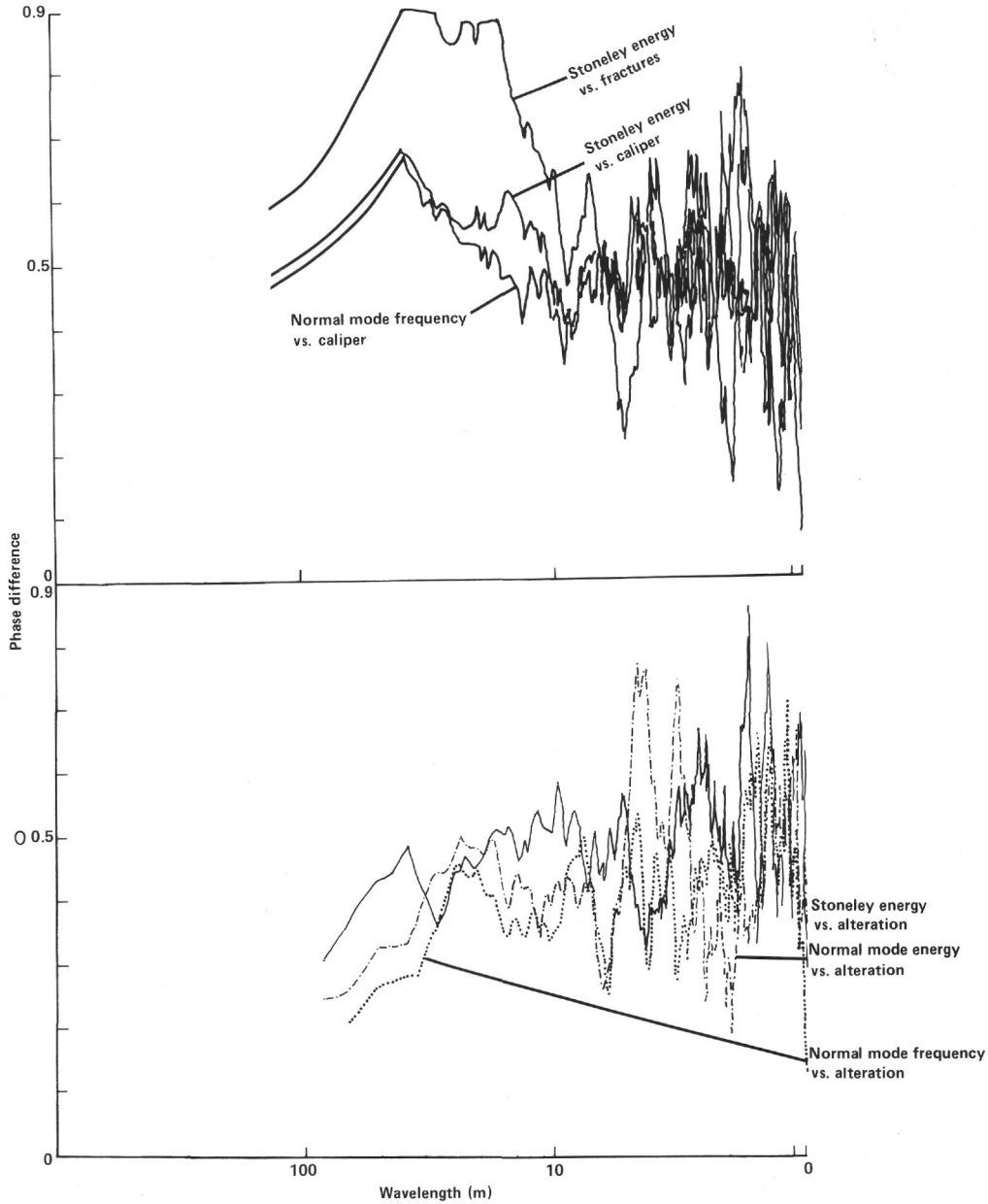


Figure 31. Phase difference of Stoneley energy against fracture log and caliper in Hole 504B, showing much stronger correlation with fractures than with hole size. Normal mode frequency shows an even weaker correlation with caliper size. Stoneley energy, normal mode energy, and frequency are correlated with alteration content below. No correlation is seen.

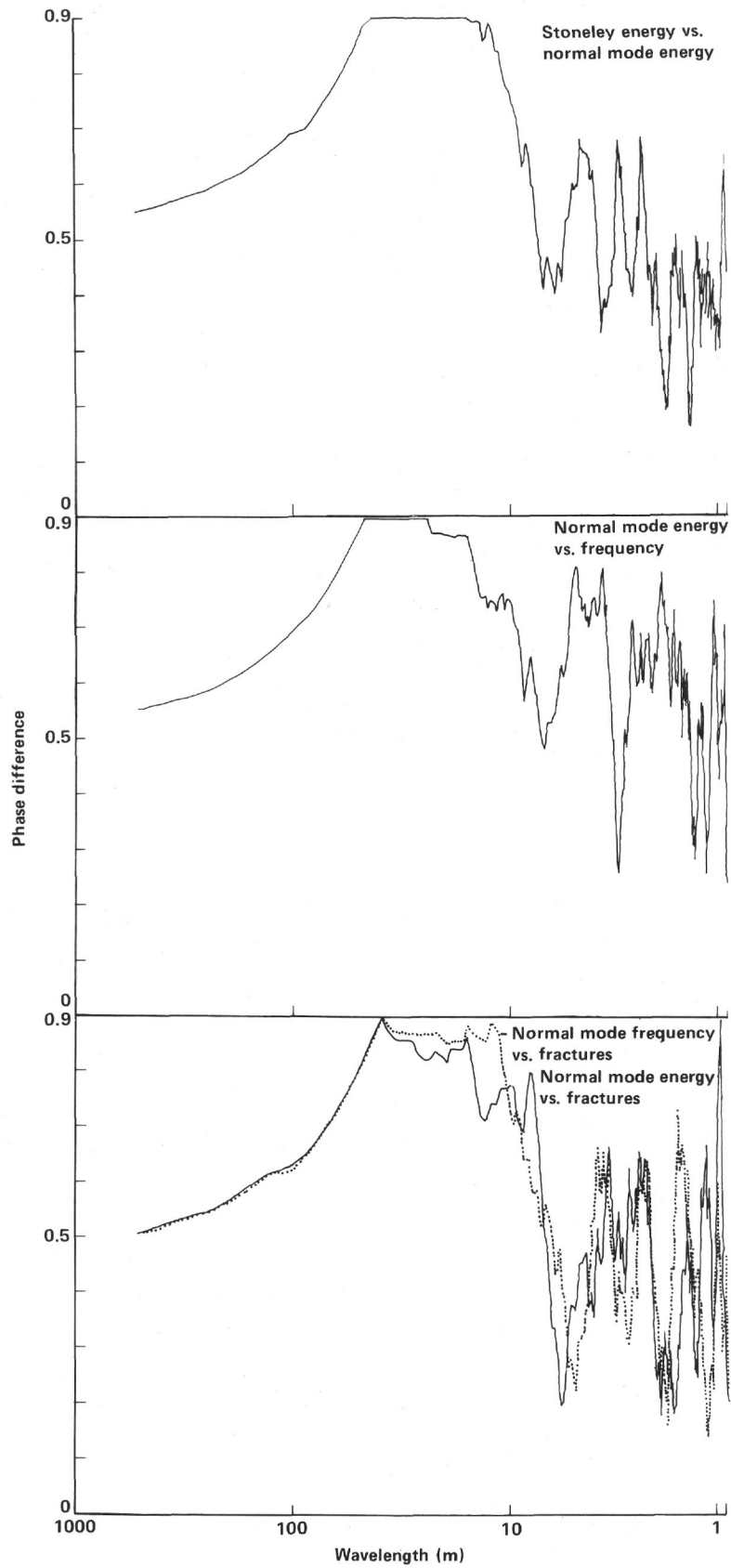


Figure 32. Phase coherence between normal mode energy and Stoneley energy, normal mode energy and frequency, and both of the latter versus fracture pattern in the bottom 150 m of the dikes in Hole 504B.

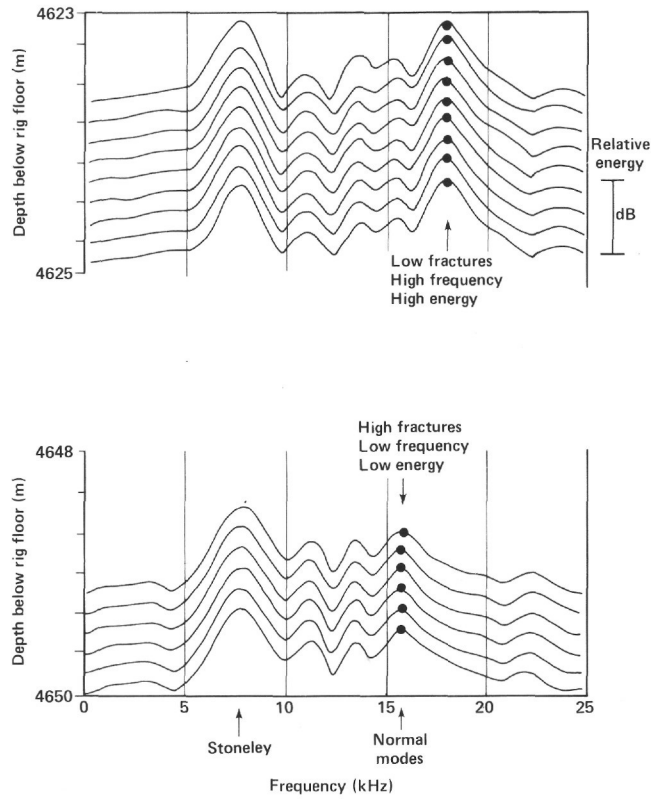


Figure 33. Actual power spectra displayed at several depths in zone with low fracture (top) and high fracture density (bottom). Energy amplitude is in dB relative to zero level at far left of each curve. Note that frequency of Stoneley wave does not change whereas energy and frequency of normal modes do.

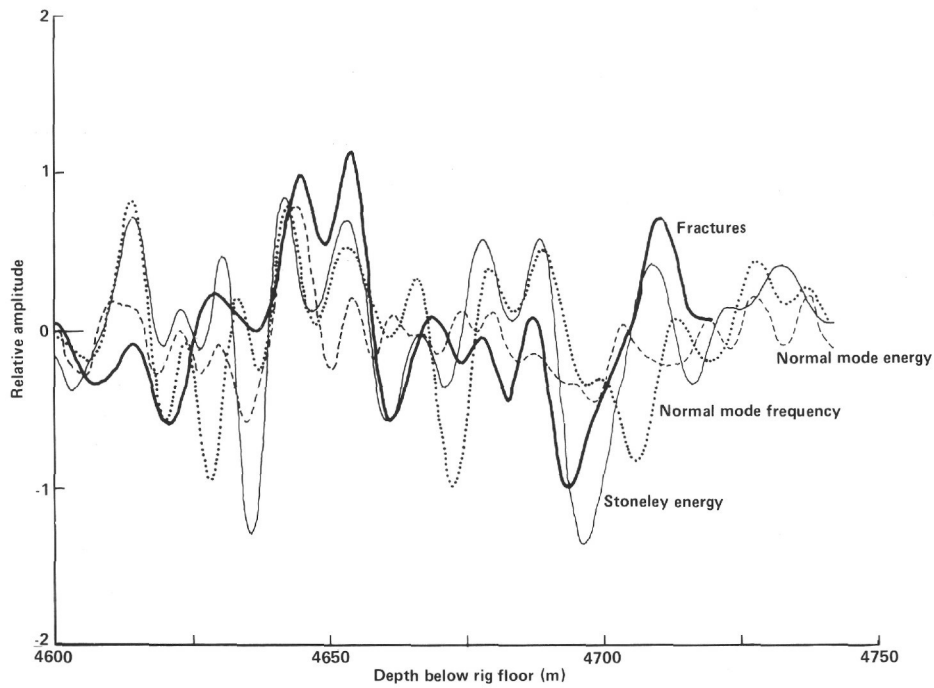


Figure 34. Detrended, normalized, and bandpass-filtered normal mode energy and frequency logs correlate with the fracture log and show pattern to fracturing in dikes of Layer 2C. The 15-25-m-thick zones of intense and highly attenuating fractures are separated by 15-25-m-thick zones of relatively solid basalt. Arrows indicate direction of increasing values of each curve.

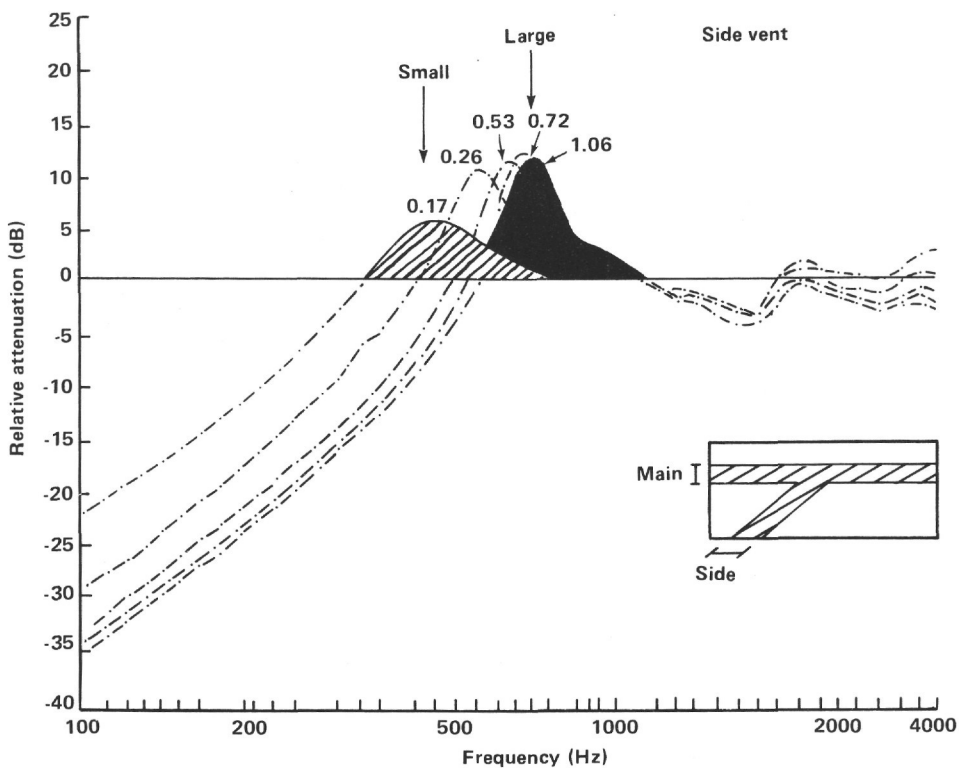


Figure 35. Experimental results from an air-filled, vented tube for variable vent constriction to main tube diameter (ratios are indicated on each curve) in lightly dampened matrix. Center or peak frequency changes and overall energy levels depend upon the vent diameter ratio. In the oceanic crust, variable vent:diameter ratios would be expected. Perhaps this phenomenon accounts for some of the scatter observed in Figures 14 and 22. If zones of intense fracturing seen in Figures 32-34 consisted of smaller-diameter vents than the solid, relatively unfractured zones, then this vent model would explain the spectral shifts observed: when fracturing is intense, with many small-diameter fractures, normal mode energy is low and frequency is also low. Zones of few fractures, each with larger diameters, would produce sections of the hole with high energy and frequency normal modes.

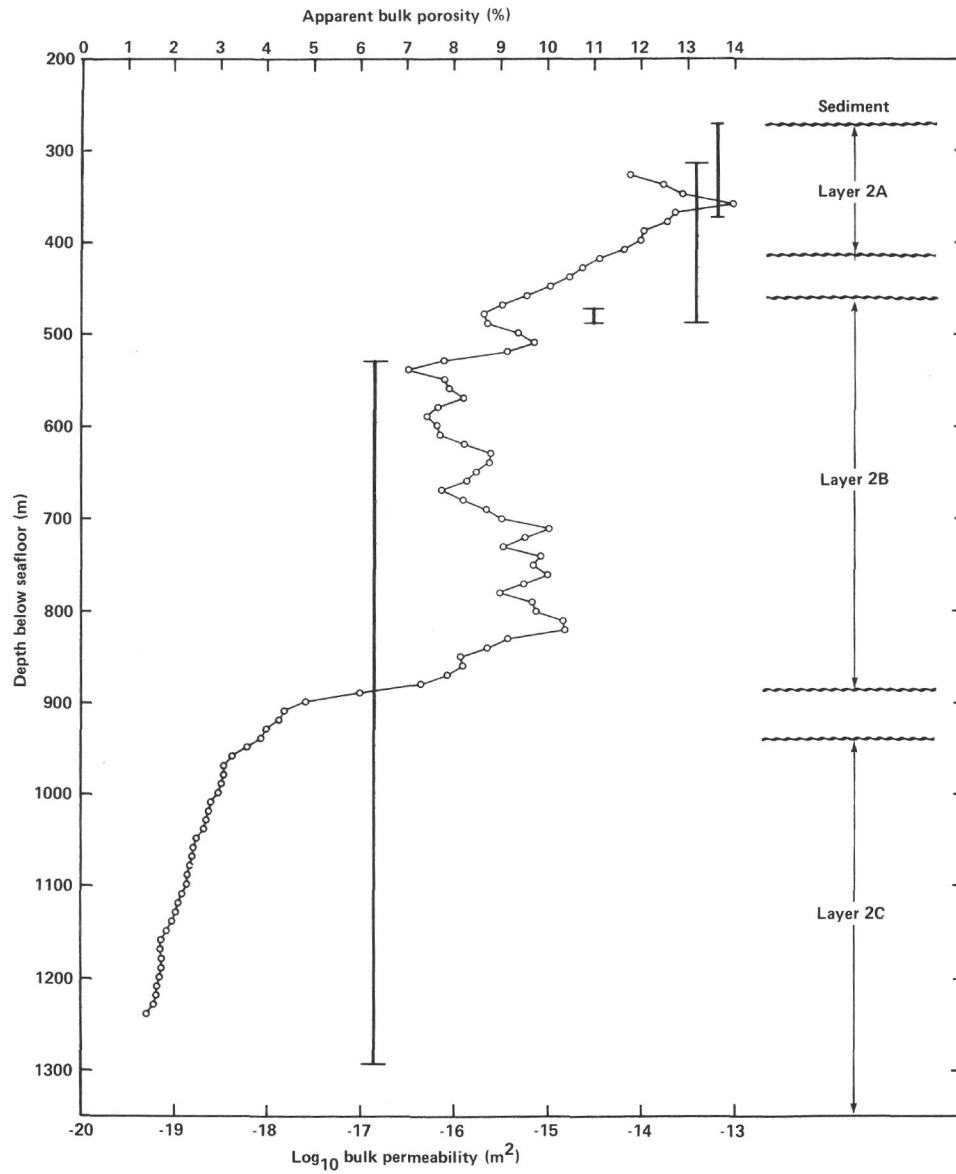


Figure 36. Apparent bulk porosity from long-spacing electrical resistivity experiment run in Hole 504B. Plotted on the same graph are permeability measurements in the same well. The two scales are not related, but the relationship between the two data trends is obvious (Becker et al., 1983; Becker, this volume). The resistivity curve would predict very low permeability in the dikes at the bottom of the hole, but the acoustic permeability of this interval is still high, implying hydraulic permeability several orders of magnitude greater than 10^{-20} m^2 (see text).